A Probabilistic Calibration of Climate Sensitivity and Terrestrial Carbon Change in GENIE-1

PB Holden[1], NR Edwards[1], KIC Oliver[1], TM Lenton[2] and RD Wilkinson[3]

1) Department of Earth Sciences
The Open University
Milton Keynes MK7 6AA

2) School of Environmental Sciences
University of East Anglia
Norwich, NR4 7TJ
and
Tyndall Centre for Climate Change Research, UK

3) Department of Probability and Statistics
University of Sheffield
Sheffield, S3 7RH

Corresponding Author:

PB Holden
p.b.holden@open.ac.uk
Telephone: +44 1908 659508
Fax: +44 1908 655151

Abstract

In order to investigate Last Glacial Maximum and future climate, we "precalibrate" the intermediate complexity model GENIE-1 by applying a rejection sampling approach to deterministic emulations of the model. We develop ~1,000 parameter sets which reproduce the main features of modern climate, but not precise observations. This allows a wide range of large-scale feedback response strengths which generally encompass the range of GCM behaviour. We build a deterministic emulator of climate sensitivity and quantify the contributions of atmospheric (±0.93ºC, 1σ) vegetation (±0.32ºC), ocean (±0.24ºC) and sea-ice (±0.14ºC) parameterisations to the total uncertainty. We then perform an LGM-constrained Bayesian calibration, incorporating data-driven priors and formally accounting for structural error. We estimate climate sensitivity as *likely* (66% confidence) to lie in the range 2.6 to 4.4ºC, with a peak probability at 3.6ºC. We estimate LGM cooling likely to lie in the range 5.3 to 7.5ºC, with a peak probability at 6.2ºC. In addition to estimates of global temperature change, we apply our ensembles to derive LGM and $2xCO_2$ probability distributions for land carbon storage, Atlantic overturning and sea-ice coverage. Notably, under $2xCO_2$ we calculate a probability of 37% that equilibrium terrestrial carbon storage is reduced from modern values, so the land sink has become a net source of atmospheric CO_2.

Keywords

climate sensitivity, Last Glacial Maximum, precalibration, structural error, emulation, GENIE-1.

1 Introduction

Climate sensitivity ΔT_{2x}, defined as the equilibrium global-mean temperature response to a doubling of atmospheric CO_2, provides the conventional measure of the change of the climate in response to increasing greenhouse gas concentrations. The best current estimate of ΔT_{2x} is that it is *likely* (66% confidence) to lie in the region 2.0 to 4.5°C (IPCC 2007), a figure which famously has changed little since Arrhenius (1886) derived the first estimate of ~5°C. The quantification of ΔT_{2x} is approached through perturbed physics ensembles (e.g. Stainforth et al 2005), multi-model ensembles (e.g. Webb et al 2006), or by constraining possible future changes with respect to known past changes (e.g. Lea 2004, Annan and Hargreaves 2006). Data and models can be combined through an observationally constrained perturbed physics experiment (e.g. Knutti et al 2002, Schneider von Deimling et al 2006); the combined approach has the advantage that whilst incorporating knowledge of previous climate states it does not assume perfect symmetry between non-analogue states, as estimates based exclusively on observational data are required to do. Here, we attempt to build upon Schneider von Deimling et al (2006), who derived a perturbed-physics estimate of ΔT_{2x} using an interval approach to constrain CLIMBER-2 with Last Glacial Maximum (LGM) tropical Atlantic Sea Surface Temperature (SST). While this approach provided an estimate for ΔT_{2x} *very likely* (90% confidence) in the range 1.2 to 4.3°C, the upper limit was increased to ~5.4°C when poorly quantified uncertainties, in particular relating to model structural error, were incorporated. Although the extent to which changes at the LGM can constrain future climate is limited by an incomplete understanding of relevant processes (Crucifix 2006), the LGM is relatively well understood, both in terms of forcing and climate, and provides an ideal model validation state, provided the uncertainties arising from model structural error are properly addressed.

We apply the model GENIE-1 (Lenton et al 2006), an intermediate complexity model built around a 3D ocean model, incorporating dynamic vegetation and sea-ice modules and coupled to an Energy Moisture Balance Model of the atmosphere. Our study complements Schneider von Deimling et al (2006), who applied CLIMBER-2, incorporating a 2.5D dynamical-statistical atmosphere coupled to a zonally averaged ocean model and fixed vegetation. Our approach does not represent an attempt to reduce uncertainty in ΔT_{2x} – an unrealistic objective in view of the greatly simplified atmospheric model and outgoing longwave radiation (OLR) feedback parameterisation – but is rather an attempt to investigate the contribution of different components of the Earth system to uncertainty in ΔT_{2x}. The use of the simplified atmosphere of GENIE-1 has the advantage that robust statistical techniques can be applied as a consequence of high computational efficiency (~3,000 model years per CPU hour in the configuration we apply here). Although much work has been done elsewhere investigating atmospheric uncertainties, in particular relating to the parameterisation of clouds (e.g. Webb et al 2006), other uncertainties, in particular those arising from vegetation, have received less attention. We note that even in cases where these processes play a minor role in ΔT_{2x} *per se*, they nevertheless represent responses to climate change which are important in their own right.

Our approach is designed to allow for the uncertainty arising from structural error e_s, the irreducible error that remains when the "best" parameter inputs are applied to a model (Rougier 2007), as distinct from the parametric error e_p that results from a non-

optimal choice of parameter inputs and which can be reduced by more careful tuning. The quantification of e_s is a highly demanding task, requiring the anticipation of the consequences of missing and/or poorly understood process and their complex interactions; Murphy et al (2007) describe an approach in which multi-model ensembles are used to derive a lower bound for e_s under the assumption that inter-model variances are likely to reflect structural error. Such an approach cannot account for structural deficiencies which are common to all models. Here we apply the concept of "precalibration" (Rougier et al in preparation), whereby the model is required only to produce a "plausible" climate state, reproducing the main features of the climate system but not constrained by detailed observations. The approach is an attempt to enable progress *without* a precise quantification of structural error; by applying only very weak constraints to the 26 input parameters which we allow to vary, and also to the modelled modern climate state we accept as plausible, we allow a wide range of large-scale feedback response strengths which generally encompass the range of behaviour exhibited by high resolution multi-member ensembles (c.f. Murphy et al 2007). We do not attempt to minimise parametric error (as would be the case in a conventional calibration) but rather deliberately allow it to dominate model uncertainty in an attempt to bypass the need for a quantification of structural error.

Computational and time constraints mean that it is not feasible to explore the entire 26 dimensional input parameter space with a naïve Monte Carlo approach. Instead, we build a computationally cheap surrogate for GENIE-1 called an emulator (Santner et al 2003) using an ensemble of 1,000 GENIE-1 model runs (described in Section 3). Only 10 of these ensemble members produced modern plausible climates (as defined above), largely as a consequence of the weak constraints imposed on parameter ranges and the corresponding sparse coverage of input space. We then apply a rejection sampling method known as Approximate Bayesian Computation (ABC) (Beaumont et al 2002) to find a collection of 1,000 parameter vectors that the emulator predicts will be modern plausible. These emulator-filtered parameterisations are then validated by performing a second modern ensemble with GENIE-1, checking that each parameter vector does indeed lead to a plausible modern climate state. Two further ensembles with LGM and doubled CO_2 boundary conditions are then generated, using the filtered input vectors, in order to investigate a range of Earth system responses (temperature and vegetation distributions, Atlantic overturning and sea-ice coverage). We discuss the range of model responses in Section 4.

In order to examine parameter interactions in setting climate sensitivity, in Section 5 we represent ΔT_{2x} through a further emulation. We use the emulator to perform a "global sensitivity analysis" (Saltelli et al 2000), apportioning variance in the output to uncertainty in the input parameters, thus providing quantification of the relative contributions of various parameterisations to the overall uncertainty in ΔT_{2x}.

To derive a probabilistic estimate for ΔT_{2x} we apply Rougier (2007) to the GENIE-1 ensemble output. The analytical approach, described in Section 6, ascribes probability weightings to the parameter vectors, constrained by observational estimates of LGM tropical SST, accounting for the uncertainty arising from structural error and incorporating prior knowledge about parameters where applicable. This enables us to derive calibrated probabilistic statements about the whole Earth System response in GENIE-1, including changes in land carbon storage, in both LGM and $2xCO_2$ states.

The calculation of climate sensitivity and sensitivity analysis is described in Section 7. The application to other Earth System responses is described in Section 8.

2 GENIE-1

We apply the intermediate complexity model GENIE-1, at a resolution of 36x36x8, in the configuration described by Lenton et al (2006). The physical model comprises C-GOLDSTEIN, a 3D frictional geostrophic ocean with eddy-induced and isopycnal mixing coupled to a 2D fixed wind-field energy-moisture balance atmosphere and a dynamic and thermodynamic sea-ice component (Edwards and Marsh 2005). The physical model is coupled to ENTS, a minimum spatial model of vegetation carbon, soil carbon and soil water storage (Williamson et al 2006). LGM Boundary conditions are as described in Lunt (2006), applying the ICE-4G LGM ice-sheet (Peltier 1994), Berger (1978) orbital parameters and an atmospheric CO_2 concentration of 190ppm. Although LGM dust forcing is neglected in the simulations, this bias is accounted for in the probabilistic analysis (Sections 6 and 7). All simulations are run to equilibrium over 5,000 years.

Two changes from Lenton at al (2006) are incorporated:

1) In order to provide realistic land temperatures for vegetation and snow cover, the effect of orography, neglected in Lenton et al (2006), is applied to surface processes by applying a constant lapse rate of 6.5×10^{-3} °Cm^{-1}. An adjustment for surface orography is not applied to atmospheric processes as these represent averages throughout the depth of the 1-layer atmosphere.

2) We assume a simple term for outgoing longwave radiation (OLR), an assumption which is discussed in some detail in Section 6. OLR at each grid cell is given by:

$$L^{*}_{out} = L_{out}(T,q) - K_{LW0} - K_{LW1}\Delta T \quad (1)$$

where $L_{out}(T, q)$ is the unmodified "clear-skies" OLR term of Thompson and Warren (1982). K_{LW0}, included to allow for uncertainty in the modern state, was allowed to vary in the range 5±5 Wm^{-2}, a range which an initial exploratory ensemble suggested was sufficiently broad to cover plausible modern output space. Positive values for K_{LW0} are assumed as the term represents a perturbation to the clear skies expression; neglecting this term lead to an underestimation of modern air temperatures by ~2-3°C in three tuned parameterisations of the model (Lenton et al 2006). $K_{LW1}\Delta T$ (Matthews and Caldeira 2007) is primarily designed to capture unmodelled cloud response to global average temperature change ΔT. The effect of this simple term for OLR, in combination with a dynamically simple atmosphere, is that all of the resulting structural error must be accounted for by uncertainty in the value for K_{LW1} which would in practice not be constant. K_{LW1} was allowed to vary from -0.5 to 0.5 Wm^{-2}K^{-1}, values suggested by an exploratory ensemble, as realistic LGM climates cannot be produced with values outside of this range. This range of K_{LW1} values suggests that the dominant processes represented by this parameter in GENIE-1 are uncertainties in cloud and lapse rate feedbacks, which approximately cancel in AOGCMs (at least in the ensemble mean) and are estimated at 0.69±0.38 Wm^{-2}K^{-1} and -0.84±0.26 Wm^{-2}K^{-1} respectively (Soden and Held 2006). We note that this cancellation may to some extent break down when latitudinal variations are considered (Colman and McAvaney

2009), so the assumption of a globally constant OLR correction will inevitably under-estimate regional uncertainty. Uncertainty in water vapour feedbacks is captured through the relative humidity threshold for precipitation, a parameter which is varied in this study, and through variability in the clear skies expression, via the uncertainty in temperature and humidity fields; in general the relationship between individual parameterisations and specific feedback strengths is not simple.

3 Precalibration of GENIE-1

Here we apply the concept of precalibration (Rougier et al in preparation) in order to develop a ~1,000 member parameter set to apply as input to three ensembles (with modern, LGM and 2xCO_2 boundary conditions). This approach, summarised in a flow chart in Figure 1, attempts to progress *without* a quantification of structural error by ruling out very bad parameter choices, but making little attempt to identify good candidates. To achieve this, we not only apply weak prior constraints to the parameters (through uniform, broad input parameter ranges) but also to the range of model output we are prepared to accept as valid; we require our model to reproduce the main features of the climate system but do not require it to accurately reproduce observations. By generating a wide spread of climate states, we assert that parametric error dominates over structural error so that we can capture the modelled uncertainty without explicitly quantifying the structural error. Analogously to Murphy et al (2007), a minimum requirement is that we can demonstrate that our ensemble encompasses the range of behaviour displayed in multi-model ensembles, a question we address in Section 4.

26 parameters were varied over the wide ranges given in Table 1. Parameter ranges were derived from the references supplied in Table 1, with minor adjustments made on the basis of an initial exploratory ensemble not described here. We define θ to be the 26-dimensional input parameter vector, and generate a 1,000 member maximin Latin hypercube:

$$D = \left\{ \theta_i^j,\ j = 1,...,1000, i = 1,...,26 \right\} \tag{2}$$

where the subscript i represents the 26 parameters and the superscript j represents the 1,000 different realisations (parameter vectors). The 26th parameter FFX does not play a role in the equilibrium calculations described here but was retained in the statistical analysis as a check for over-fitting.

The parameter set D was applied as input to an initial modern ensemble of GENIE-1. The purpose of this initial ensemble is to provide the data required to build five emulators of modern climate. These emulators are computationally cheap (polynomial) relationships between the 26 input parameters and the five selected model output diagnostics. The output diagnostics are designed to test the ocean (Atlantic overturning strength), atmosphere (global average Surface Air Temperature, SAT), sea-ice (annual average Antarctic sea-ice area) and land carbon storage (total vegetative carbon and total soil carbon). We subsequently apply these emulators to design the parameter set applied to the ensembles described in subsequent sections.

Before building the emulators, the five modern plausibility tests were applied to the output of the GENIE-1 ensemble. The required ranges are summarised in Table 2 ("plausibility test R_k"). These ranges are substantially broadened from observational uncertainty in order to allow for model structural error and ensure that the range of plausible model outcomes contains the "true" climate state. The ranges selected for precalibration filtering are model dependent (Rougier et al in preparation) as, for instance, low resolution model outcomes would be tend to be viewed more leniently. We define $f(\theta)$ to be the 5-dimensional summary (the plausibility characteristics) of GENIE-1 run at θ. A parameter vector was considered modern plausible only if *all five* of the plausibility metrics fell within the accepted ranges:

$$\left| f_k\left(\theta^j\right) - \mu_k \right| \le \varepsilon_k \qquad \text{for } k = 1, \ldots, 5 \tag{3}$$

where μ_k are the mid points and ε_k the half widths of the plausibility ranges R_k in Table 2. In this initial ensemble only 10 of the simulations were found to provide a plausible modern climate state for all five constraints simultaneously, reflecting the broad parameter ranges supplied and consequent under-sampling of input space.

In order to produce a large plausibility-constrained parameter set, deterministic emulators ζ_k were built for each of the five metrics, following Rougier et al (in preparation), performing stepwise logistic regression, including linear, quadratic and cross terms for all 26 variables. (The ΔT_{2x} emulator, described in Section 5, additionally includes cubic terms, thus allowing three-way interactions). Prior to fitting, variables were linearly mapped onto the range [-1, 1] so that odd and even functions are orthogonal, improving the selection of terms. Stepwise selection was performed using the stepAIC function (Venables and Ripley 2002) in R (R Development Core Team 2004), minimising the Akaike Information Criterion (which attempts to best explain the data with the minimum of free parameters). Terms were subsequently removed by applying the more stringent Bayes Information Criterion (which penalises free parameters more strongly). Three of our chosen 26 parameters can have no role in the modern state: OL1 (K_{LW1} in Equation 1), VPC (describing the CO_2 fertilisation of photosynthesis and normalised to a modern response at 280ppm) and the dummy variable FFX; the final models were pruned by selecting a significance threshold sufficient to eliminate these three parameters from the emulators and minimise overfitting.

In order to investigate the role of individual parameters in determining a plausible modern state, a global sensitivity analysis (Saltelli et al 2000) was performed for each emulator, calculating the contribution of each parameter to the variance of that emulator. For each of the emulators ζ_k, we calculate the *total effect* V_{kT} of θ_i. This represents the remaining uncertainty in $\zeta_k(\theta)$ after we have learnt everything except θ_i i.e. the expected variance of $\zeta_k(\theta) \mid \theta_{[-i]}$, where $\theta_{[-i]} = (\theta_1,\ldots,\theta_{i-1}, \theta_{i+1},\ldots, \theta_n)$:

$$V_{kT_i} = E_{[-i]} Var_{\theta_i}\left(\zeta_k(\theta) \mid \theta_{[-i]}\right) = \iint \left(\zeta_k(\theta) - E\left(\zeta_k(\theta) \mid \theta_{[-i]}\right)\right)^2 d\theta_i d\theta_{[-i]} \tag{4}$$

which is readily solved analytically for the polynomial emulators and uniform prior distributions considered in this section.

Figure 2 plots the total effect of each parameter (normalised to a total of 100%) for each of the emulators, thus illustrating the relative importance of each parameter in controlling the five plausibility metrics. The emulators exhibit an R^2 of 98% (SAT), 88% (Atlantic overturning), 91% (Antarctic sea ice area), 98% (vegetative carbon) and 94% (soil carbon) with respect to the simulated output, and thus provide a reasonably accurate description of the apportionment of variance of GENIE-1. It is important to note that the total effect depends upon the range across which the parameter is allowed to vary, and consequentially it is a subjective measure, dependent upon the expert judgement applied in determining these ranges.

1) Uncertainties in global average SAT are dominated by uncertainties in OL0 (primarily the effect of cloud uncertainty on the modern-day radiation balance), RMX, the relative humidity threshold for precipitation (through its influence on the water vapour feedback), AHD, the atmospheric heat diffusivity, and VFC, defining the dependence of fractional vegetation coverage on vegetation carbon though its control on land surface albedo.

2) In GENIE-1, uncertainties in Atlantic overturning are dominated by the atmospheric transport of freshwater through APM, the Atlantic-Pacific freshwater flux adjustment (which corrects for the ~0.29Sv underestimation of atmospheric moisture transport from the Atlantic to the Pacific and is required for a stable Atlantic overturning, Edwards and Marsh 2005) and AMD, the atmospheric moisture diffusivity. Ocean tracer diffusivities (OHD and OVD) and the ocean drag coefficient (ODC) also play a significant role.

3) Uncertainties in sea-ice, though substantial, are not dominated (in GENIE-1) by the sea-ice parameterisations themselves, but rather by the parameterisations of atmospheric and ocean transport, and exhibit a close coupling with parameters that control global average temperature and the equator-pole temperature gradient.

4) Although uncertainties in vegetation are largely controlled by parameters which exert control on the rate of photosynthesis (notably VBP, the base rate of photosynthesis, and VFC) and the leaf litter rate (LLR), atmospheric transport through heat diffusivity (AHD) and moisture diffusivity (AMD) also play an important role.

5) Uncertainty in soil carbon is dominated by the parameterisation of soil respiration through SRT, the activation temperature for soil respiration, and SRR, the soil respiration rate, although the parameters which control the source of soil carbon, through the production of vegetation carbon and ultimately leaf litter, play a significant role.

We used these emulators as a cheap surrogate for GENIE-1 in order to perform the precalibration. An Approximate Bayesian Computation (ABC) method (Beaumont et al 2002) was applied to the emulators. This procedure updates the uniform prior distribution for θ (Table 1) in light of the emulated plausibility metrics $\zeta_k(\theta)$ to find a posterior distribution for θ. This is accomplished by drawing parameters randomly from their defined input ranges and accepting them as potentially valid if the emulators reproduce observations to within an acceptable level on each of the plausibility measures:

$$\left|\zeta_k(\theta) - \mu_k^*\right| \leq \varepsilon_k^* \quad (5)$$

where μ_k^* are the mid points and ε_k^* the half widths of the ABC ranges R_k^* in Table 2. For the purposes of ABC filtering, accepted ranges were narrowed from the plausibility ranges R_k. This is partly to avoid unnecessary wastage caused by imperfect emulation of the model and partly, given emulator error, to ensure the ensemble average output is centred close to observations, in order to minimise potential bias in the modern state (on the assumption that our expectation of structural error has zero mean). This process was continued until we had accepted 1,000 values of θ. The resulting set is labelled P. This required sampling ~12 million randomly generated values of θ, illustrating the necessity for emulation (or alternatively a very much more efficient sampling procedure). We note that although we describe this process as a precalibration, rather than a calibration, this distinction simply reflects the broad ranges we have applied for ABC filtering.

Next we perform a second ensemble of GENIE-1 simulations with the emulator-predicted plausible set of 1,000 parameter vectors P and apply the plausibility test to the simulated values $f_k(P)$ (Equation 3). P was found to contain 944 members which satisfied all five modern plausibility requirements in the simulations. These 944 plausible members of P were applied to two further ensembles with LGM and 2xCO_2 boundary conditions. 894 of the LGM runs completed successfully and did not exhibit runaway LGM cooling (as defined by LGM Antarctic SAT > 20°C cooler than modern). These form the parameter set we call *"Modern plausibility constrained" (MPC)*, though noting that this is a slight misnomer as a very weak LGM filtering has been applied in addition to the modern constraints. A further plausibility constraint was applied, derived from the LGM ensemble and requiring Antarctic SAT to be between 6 and 12°C cooler than modern (c.f. Antarctic LGM SAT anomaly 9±2ºC, Crucifix 2006). 480 of the MPC parameter vectors satisfied this criterion and form the *"LGM plausibility constrained" (LPC)* parameter set. In summary, the MPC parameter set represents the 894 parameterisations which are modern plausible and the LPC parameter set represents the 480 member subset of these which additionally satisfy LGM plausibility.

The standard deviations and ranges of the GENIE-1 ensemble output are provided in the final two columns of Table 2. These characteristics are derived from the MPC parameter set, though to the significance quoted the averages and 1σ statistics apply equally to the LPC parameter set; the LGM plausibility test has neither constrained nor biased the modern state. Although our decision to narrow the ABC filtering range may have constrained vegetative carbon more than is ideal for these purposes, the approach has achieved our objective of generating a large number of weakly constrained parameter vectors, over broad input ranges, which produce a wide range of plausible climate states, approximately centred on modern observations.

4 Plausibility Constrained LGM and 2xCO2 climate states

Our statistical approach requires that the ensemble covers the range of large-scale behaviour exhibited in multi-model GCM ensembles (accepting inevitable differences in the spatial feedback structure and in the contribution of individual feedbacks to the total feedback strength between the GENIE-1 ensemble and GCMs). We here

investigate the variability in our ensemble of modern climate, and in the response to LGM and $2xCO_2$ boundary conditions.

The LPC ensemble-averaged distributions of modern SAT and of LGM and $2xCO_2$ SAT anomalies are plotted on the left hand column of Figure 3. The corresponding standard deviation fields are plotted on the right. The modern temperature distribution is generally reasonable, with the exception that average Antarctic temperature is ~10°C cooler than NCEP data; GENIE is known to underestimate Antarctic sea-ice (Lenton et al 2006) and enforcing plausible Antarctic sea-ice coverage may have introduced this cold Antarctic bias. Average LGM Antarctic cooling of 8.3±1.6°C is consistent with ice core estimates; the MPC ensemble members, not constrained for LGM plausibility, exhibit an Antarctic temperature anomaly of 7.7±3.0°C.

Similarly to Schneider von Deimling (2006) the largest SAT variability is associated with Southern Ocean and Northern Atlantic sea ice. The dynamic vegetation module introduces additional uncertainty over land, especially at high northern latitudes. This is largely driven by the strong dependence of snow covered albedo on vegetational coverage. Although we do not vary the parameterisation of snow covered albedo in this study, uncertainty nevertheless arises through the variability of vegetative carbon density (see Williamson et al 2006, Equation 31). GENIE-1 generally exhibits greater variability than the CLIMBER-2 ensemble of Schneider von Deimling (2006), because we have used an approach which deliberately covers a wide range of uncertainty in the modern state. Notwithstanding this, variability will inevitably be underestimated due to the absence of a dynamical atmosphere.

To further investigate the exhibited range of climate response, we consider polar amplification, defined as the ratio between Greenland / Antarctica and global annual mean temperature change. In Antarctica, a similar polar amplification is simulated under both LGM forcing (1.4 ± 0.2 (1σ), *cf* 0.9 to 1.6) and $2xCO_2$ forcing (1.8 ± 0.2, *cf* 1.1 to 1.6); quoted comparative ranges are the 25th-75th percentiles from elevation-corrected PMIP2 comparisons (Masson-Delmotte et al 2006). In Greenland, polar amplification is substantially greater under LGM forcing (2.4±0.4, *cf* 1.9 to 2.6) compared to $2xCO_2$ forcing (1.2±0.2, *cf* 1.2 to 1.6), reflecting the greater influence of Northern Hemisphere ice sheets on Greenland temperatures. Although the GENIE-1 ensemble characteristics are similar to those of the multimodel comparison, the slightly lower variability displayed by GENIE-1 is at least in part a consequence of the globally constant value applied for the OLR parameterisation (Equation 1), in addition to the lack of dynamic 3D structure.

Figure 4 plots the spatial distribution of vegetative carbon (not including soil carbon). The average modern vegetative carbon distribution is reasonable, especially considering the broad parameter ranges and the single constraint that has been applied to total vegetation carbon. The main problems, a lack of distinct desert regions (due to an over-diffusive atmosphere) and an underestimation of boreal forest (due to restricted moisture transport into the continental interior) were also found by Lenton *et al* (2006). Approximately 50% of vegetative carbon is located in tropical latitudes (30°N to 30°S), lower than observational estimates of ~60% (Olsen et al 1985). The largest uncertainty in vegetative carbon is associated with tropical vegetation.

In LGM conditions the largest vegetation changes are driven simply by the removal of vegetation under the ice sheets. Away from the ice sheets, the largest changes and greatest uncertainty are associated with a reduction in tropical carbon, though significant variability is associated with high latitude vegetation.

In the $2xCO_2$ state, the average response is increased vegetative carbon at all latitudes, though 4% of simulations show a reduction in vegetative carbon and 20% show a reduction in total land carbon storage (vegetation *and* soil) due to increased heterotrophic respiration at elevated temperature; our range for SRT (Table 1) is equivalent to a Q10 range (the increase in respiration rate for a 10°C temperature increase) of 1.4 to 3.2. Although the greatest increases in vegetative carbon are at high latitudes, the greatest variability is at low latitudes where the competing effects of increased photosynthesis and increased respiration rates can result in NPP reduced relative to modern levels; 23% of the simulations show a reduction in tropical vegetative carbon (and 49% a reduction in tropical land carbon storage). This equilibrium behaviour is qualitatively similar to that exhibited by a range of transient (1850-2100) simulations using eleven coupled climate-carbon cycle models (Friedlingstein 2006). These models universally exhibited increased land carbon storage under elevated CO_2 (though two models simulated a sink/source transition for land carbon flux by 2100), with increased uptake due to CO_2 fertilisation dominating over a climate-change driven reduction in uptake-efficiency. These simulations also displayed increased variability in tropical vegetation, possibly a consequence of the moisture dependence of tropical NPP dominating over the temperature dependence and the difficulties in simulating the hydrological cycle. The lack of a dynamic atmosphere in GENIE-1 is likely to result in an underestimate of the uncertainty associated with the hydrological cycle; notably the large scale tropical desertification simulated by HadCM3 is not apparent in any of the GENIE-1 simulations. We note that our ensemble averaged response is likely to overestimate the effect of CO_2 fertilization due to the wide ranging input values of VPC, a parameter which is not constrained by modern plausibility; the effect of introducing a data-derived prior to constrain this response is discussed in subsequent sections.

Figure 5 contains similar plots for the Atlantic overturning stream function. Pre-industrial overturning peaks at 18±3Sv at a depth of ~0.8km. The formation of NADW (as defined by the 10Sv contour) is located at ~57°N. These figures are similar to a range of 9 PMIP simulations (Weber 2007), which exhibit 20±4Sv, 1.0±0.2km and 62±3°N, respectively. The major shortcoming of GENIE-1 in this configuration is the failure of AABW to penetrate into the Atlantic sector (Lunt et al 2006), possibly related to the neglect of thermobaricity (the effect of pressure on the thermal expansion coefficient) in the equation of state. The peak average LGM overturning is slightly stronger than modern (~19±3.0Sv) and occurs at a similar depth to modern (~0.8km) though it extends to greater depths. The formation of NADW is shifted southward to ~53°N. These figures compare with PMIP averages, which also exhibit substantial variability in the LGM stream function (with unclear change of sign), to values of 20±5Sv, 1.1±0.4km, 55±9°N (Weber 2007). The average $2xCO_2$ overturning has a similar spatial distribution to the pre-industrial, but exhibits a slight weakening to an average of 17±4Sv.

Figure 6 compares the MPC frequency histograms for each of the five plausibility diagnostics, illustrating both LGM and $2xCO_2$ anomalies. In contrast to Figures 3-5,

these histograms are not filtered for LGM plausibility in order to illustrate the complete GENIE response. We note that for ease of presentation a small number of "outlying" (though important) data points are not plotted; these extreme responses are discussed in the text. These histograms represent the precalibrated sensitivity of GENIE-1, in contrast to the calibrated calculations derived later in Sections 6-8.

In these distributions, the $2xCO_2$ global air temperature anomaly (i.e. the precalibrated GENIE-1 climate sensitivity) peaks at ~3.0 °C and the LGM anomaly at ~ -4.0°C. We note that GENIE-1 does not generate ΔT_{2x} below ~2.0°C at any point in our input parameter space. Although sufficiently low values of K_{LW1} can generate arbitrarily low (positive) climate sensitivities, values outside of our input range are difficult to reconcile with the LGM plausibility constraint. In initial exploratory ensembles, only 15 from 249 parameterisations with K_{LW1} in the range -0.5 to -1.0$Wm^{-2}K^{-1}$ resulted in an LGM Antarctic anomaly >6°C and none of these 249 parameterisations produced an anomaly >9°C (*cf* observational estimate 9±2°C, Crucifix 2006). Notwithstanding this, some caution should be exercised in interpreting our lower bound estimate for ΔT_{2x}, especially given that the neglect of dust is likely to have resulted in an Antarctic warm bias of ~1°C (Schneider von Deimling et al 2006b). Furthermore, we note that lower values of ΔT_{2x} could be generated if the assumption of a constant feedback parameter for LGM and $2xCO_2$ states breaks down, as is very likely the case (Crucifix 2006); we discuss this assumption further in Section 6 and account for it by incorporating an explicit structural error term in Section 7.

The LGM-modern anomaly in Atlantic overturning (defined as the maximum overturning stream function at depths below ~400m) peaks at ~2 Sv. Although the distribution reflects a preference in GENIE-1 for a strengthened LGM overturning, 29% of the simulations exhibit a weakened LGM overturning. It is well known (Weber 2007) that models disagree on the sign of this change, reflecting a balance of competing freshwater and temperature effects on the density distribution. It is interesting that this uncertainty in sign is demonstrated by a single model, suggesting that much of this disagreement may be arising from parametric uncertainty and therefore may not reflect a fundamental difference between the models themselves. In a $2xCO_2$ state, the distribution reflects a strong preference for a slight weakening of overturning. Nine of the 894 simulations exhibited a collapse of the Atlantic overturning in a $2xCO_2$ state (as defined by <10% of modern overturning strength). We note that as we do not allow for the possibility of a Greenland meltwater contribution to the freshwater balance, we are likely to underestimate the probability of collapse, and the magnitude of weakening in general. Conversely, four of the simulations exhibit a substantial strengthening of Atlantic overturning (~5-10Sv), though in each case the modern distribution is unrealistic, shifted very far southwards to ~25°N with greatly weakened North Atlantic deep convection.

The increase in annually-averaged LGM sea-ice area peaks at ~9 million km^2 in the Antarctic and ~7 million km^2 in the Arctic, though substantial uncertainty is exhibited. In a $2xCO_2$ state, sea-ice loss peaks at ~6 million km^2 in the Antarctic and ~3 million km^2 in the Arctic. The small probability of an increase in Arctic sea ice is associated with the occasional collapse of Atlantic overturning and the associated reduction of northward heat transport. The Arctic remains ice-free throughout the year in ~5% of the $2xCO_2$ simulations, at least in part due to our low resolution, though

these parameterisations are all associated with low sea-ice cover in the modern state (with an annual average of 4.4 million km^2).

LGM reductions in vegetative carbon ~150 GtC and soil carbon ~450 GtC are consistent with a range of data and model estimates (Peng et al 1998) of ~30% reduction in land carbon storage. Although the $2xCO_2$ distribution of vegetative carbon strongly favours an increase from modern values (with only 4% simulations exhibiting a reduction), the soil carbon distribution reflects change of an unclear sign (with 29% of simulations exhibiting a reduction), driven by competing effects of an increased source (vegetation carbon) and increased respiration rates in a warmer world. The MPC distribution for total land carbon storage change under doubled CO_2 is 250±294 GtC,

In summary, we have demonstrated that our experimental design has produced an average climate state that is reasonably well centred on modern observations, but which exhibits a wide range of responses to both LGM and $2xCO_2$ forcing, a range which encompasses much of the differing behaviour that is observed in more complex models.

5 An Emulation of Climate Sensitivity

In order to investigate the interactions between parameters and to quantify the contribution of the individual parameterisations to climate sensitivity in GENIE-1, we built a deterministic emulator for ΔT_{2x}, following the procedure described in Section 3. The emulator was built from the MPC parameter set; the LGM plausibility constraint was not applied in order to maximise the range of the response. After an initial emulation was performed including quadratic terms for all 26 parameters (the *quadratic emulator*), the 6 parameters which did not exhibit significant interactions were excluded and the complexity of allowed emulator interactions increased to include cubic terms (the *cubic emulator*). The cubic emulator exhibited a standard error (the standard deviation of the discrepancy between emulated and simulated climate sensitivity) of ±0.12°C and an R^2 of 97.4%. As a check against over-fitting, a second cubic emulator (*cubic_600*) was built with an identical methodology but from a random subset of 600 of the MPC parameter vectors. The remaining 294 members were used as a validation set, and displayed a bootstrapped standard error of ± 0.16°C. The R^2 between the 85 coefficients of the cubic emulator and their equivalent coefficient (zero if absent) in the cubic_600 emulator is 71%, suggesting the dominant terms can be regarded as a reasonably robust representation of GENIE-1.

The emulators allow us to investigate the uncertainty in ΔT_{2x} as a function of the input parameters. As in Section 3, we achieve this through a global sensitivity analysis, calculating the total effect of each parameter, which provides a measure of the contribution of that parameter to the variance in emulated climate sensitivity (Equation 4). We do not calculate the total effect analytically (as in Section 3) but approximate the integral by averaging over the Latin Hypercube (D) and over the LPC parameter set (Table 3). The Latin Hypercube calculation describes the apportionment of variance given the initial uniform independent prior ranges summarised in Table 1. The LPC calculation illustrates the constraining effect of modern plausibility. Table 3 summarises the Latin Hypercube calculation under various assumptions. The main result is the 1st data column (in bold) which tabulates

the square root of the total effect (as a measure of the 1σ variation) in the cubic emulation. The following three columns test the robustness of this result by calculating the total effect for i) the cubic emulator over a subset of 500 of the Latin Hypercube members (to test for convergence of the approximate calculation of V_{kT}), ii) the cubic_600 emulator and iii) the quadratic emulator. Integrating the emulator over uniform priors requires extrapolating beyond the narrow plausible regions (of 26-dimensional space) that were used to train the emulator. However, these four calculations all provide similar results, suggesting the apportionment of variance to the parameters is robust. The similar results for the cubic and quadratic emulators suggest that three-way interactions are not significant. We note that the emulators achieve this similar apportionment of variance through different combinations of cross-terms, suggesting that the details of the individual interactions may be difficult to interpret unambiguously.

Interactions introduced in the MPC parameter set through the enforcement of modern plausibility introduce correlations between parameters. In general these are weak, but three parameter pairs are highly correlated: OL0/RMX (R^2=74%, negatively correlated as increases in either leads to reduced OLR, with similar effects on modern SAT plausibility), SRT/SRR (R^2 = 34%, positively correlated through their opposing effects on soil carbon) and AMD/APM (R^2 = 30%, positively correlated through their competing effects on North Atlantic surface salinity and hence on Atlantic overturning). As a consequence, the apportionment of variance between these paired parameters may not be robust. Notably, we cannot rule out the possibility that all of the uncertainty ascribed jointly to OL0 and RMX ($\sqrt{\Sigma V_T}$ = 0.30°C) is driven entirely by uncertainties in RMX; physical considerations suggest OL0 is unlikely to contribute to uncertainty in climate sensitivity as it represents OLR uncertainty in the modern state (Equation 1) and has no clear feedback role (whereas RMX exerts influence on the water vapour feedback by limiting relative humidity). However, as all three parameter pairs are within the same module (atmosphere, vegetation and atmosphere respectively), this does not affect the apportionment of uncertainty between modules discussed below.

This procedure ascribes 85% of the variance to the EMBM parameters, associated with an approximate 1σ error of ±0.93°C (Table 3, calculated as $\sqrt{\Sigma V_T}$ summed over the EMBM parameters, and providing an upper bound as the summed total effect is always greater than the total variance). Although dominated by atmospheric processes, the variance associated with other modules indicates that they are not negligible and contribute approximate 1σ errors of ±0.32°C (vegetation), ±0.24°C (ocean) and ±0.14°C (sea-ice). Note the low uncertainty associated with sea-ice parameterisations does not imply a weak sea-ice feedback; uncertainty in the sea-ice feedback is dominated by uncertainties in sea-ice area which in turn are dominated by uncertainties in ocean and atmospheric transport rather than the sea-ice parameterisations themselves (see Fig. 2). In general, it is not trivial to associate particular parameterisations with individual feedback mechanisms.

Figure 7 plots the dominant emulator interactions. Only parameters which contribute more than 1% to the total variance were considered and only interactions large enough to change the emulated climate sensitivity by more that the standard error are included. A single three-way interaction (OHD:OL1:LLR) was additionally excluded as this interaction was not present in the cubic_600 emulator and thus may not be

considered robust when viewed in isolation. The strong interactions plotted are unlikely to represent an over-fitting to the model output, though we cannot rule out the possibility that the correlations in input space noted earlier may influence these interactions. It is apparent that the strongest inter-module interactions (controlling climate sensitivity) take place through the EMBM. The dominant parameter is OL1, which crudely parameterises the role of cloud and lapse rate feedbacks. Atmospheric moisture diffusivity is notable in that it does not affect climate sensitivity directly (i.e. through a linear term), but is strongly coupled to the rest of the system and, in particular, interacts strongly with feedbacks in vegetation and atmospheric humidity.

6 Introducing a probabilistic LGM data constraint

In order to calculate posterior probability distributions for climate, we first derive posterior probability weightings for the parameter vectors by applying an LGM constraint and subsequently apply these weightings to the precalibrated distributions of Figure 5; note this calibration is performed upon the simulator (GENIE-1) output, not the emulated output. This section describes the analytical approach, including a discussion of the base case (Section 7, Assumption A7) structural error assumptions applied. The calculation of climate sensitivity, including a sensitivity analysis to the structural error assumptions is performed in Section 7.

The approach follows Rougier (2007) throughout. We denote the true climate state by the vector y, measurements of climate by the vector z and model estimates of the climate by the vector $g(\theta)$, where θ is the 26 dimensional input parameter vector. We take the best input approach (Rougier 2007) and assume that there is a value of θ, denoted θ^*, such that $g(\theta^*)$ is the best possible prediction of the true climate state y. We relate observations, climate and best model prediction by the following relationships

$$z = y + e_o \tag{6}$$

and

$$y = g\left(\theta^*\right) + e_s \tag{7}$$

where e_o and e_s represent measurement and model error respectively, The aim is then to find the posterior distribution of θ^* in light of the LGM tropical SST anomalies.

We model both the model and measurement error terms as Gaussian random variables. For e_o we use a zero-mean Gaussian distribution with variance σ_o, whereas for the model error we allow the possibility of a bias in the model predictions and assume that e_s has a Gaussian distribution with specified mean μ and variance σ_{LGM}. While the Gaussian assumption is common for observation error, it is more difficult to justify for the model error term. We follow Rougier (2007) and make this assumption for reasons of tractability, rather than for any strongly held belief that the error is normally distributed. Note that this represents an improvement over standard practice, where it is usual to assume that $\sigma_{LGM} = 0$ which is equivalent to the assumption that the model is perfect.

We update the prior distribution in light of the LGM constraint z_{LGM} to find the posterior distribution, using Bayes' theorem (Rougier (2007), Eq. 7):

$$\Pr\left(\theta^* \mid z_{LGM} = \tilde{z}_{LGM}\right) = c\varphi\left(\tilde{z}_{LGM} - g_{LGM}\left(\theta^*\right); \mu; \sigma_o + \sigma_{LGM}\right) p\left(\theta^*\right) \quad (8)$$

where $\varphi(.)$ is the Gaussian density function with specified mean and variance, and c is a normalising constant.

For the LGM constraint, we apply the result of the Bayesian multi-proxy analysis of Ballantyne et al (2005) for tropical SST anomalies of 2.7±0.5°C. i.e $\tilde{z}_{LGM}$ (observed LGM tropical SST anomaly) = 2.7°C, $\sqrt{\sigma_o}$ =0.5°C, where $g_{LGM}(\theta^*)$ is the modelled LGM tropical SST anomaly with error (μ, σ_{LGM}). The choice of a tropical SST constraint is discussed in some detail in Schneider von Deimling (2006), favoured by well-calibrated proxy data, large scale averaging (minimising the influence of local processes which cannot be captured by our coarse resolution fixed wind-field model) and a signal which is less affected by uncertainties in the topography of Northern hemisphere ice sheets.

An equal prior probability is ascribed to all LPC plausible parameter vectors $p(\theta)$ (with a zero probability ascribed to the other parameter vectors); this does not represent a simple uniform prior probability across θ space as the plausibility filtering has already imposed constraints upon parameters and upon the interactions between parameters; i.e the posterior distribution from the plausibility filtering forms the basis for our prior assumption here. These priors are further adjusted by two data-driven estimates. VPC is constrained by the compilation of CO_2 fertilisation data of Wullscheleger et al (1995) which implies a Gaussian distribution of $\varphi(145, 200)$ ppm for the Michaelis-Menton half saturation; plausibility tests do not constrain this response and the photosynthesis data suggest the lower end of our input range (0 to 700ppm) should be favoured. A prior is applied for oceanic isopycnal diffusivity, also poorly constrained by modern plausibility, assumed to be a gamma distribution (α=2, β=1000) m^2s^{-1}, exhibiting a mode of 1,000 m^2s^{-1} and a mean of 2,000 m^2s^{-1}. Our choice of mode represents the canonical value for vertically constant isopycnal diffusivity (as applied here), though this value is associated with substantial uncertainty and spatial variability (Ferreira et al 2005).

The neglect of dust is a major source of structural error in the LGM SST anomaly σ_{LGM}; the main effect of LGM dust was a likely cooling in the tropics (Claquin 2003). Schneider von Deimling (2006) incorporated dust fields and implied an additional tropical SST cooling of 0.4 to 0.9°C. As the absence of dust introduces a bias, as well as an uncertainty, we incorporate this by applying a non-zero mean μ of 0.6°C to the structural error, in addition to $\sqrt{\sigma_{LGM}}$ = 1.0°C. Though we describe the absence of a coupled dust model as a source of structural error, we note that it could equally be described as an absent forcing; the analytical approach is not affected by this distinction.

A probability distribution for climate sensitivity $y_{\Delta T_{2x}}$ can then be found using the law of total probability (Rougier (2007) Eq. 8), which we approximate by a Monte Carlo estimate. Although some aspects of structural error may covary between different climate states, we lack sufficient information to estimate all possible sources of

structural error and assume for tractability that the net covariance between the paleo-climate and future climate state, in both measurement error and structural error, is zero (see Rougier 2007, Section 6.3). In this case

$$\Pr\left(y_{\Delta T_{2x}} \mid LGM\right) = \sum_{LPC} \varphi\left(y_{\Delta T_{2x}} - g_{\Delta T_{2x}}\left(\theta^*\right); \mu_{CS}; \sigma_{CS}\right) \Pr\left(\theta^* \mid LGM\right) \quad (9)$$

where we sum over the LPC parameter set, applying the posterior probabilities *Pr(θ|LGM)* derived in Equation 8. Here we have assumed the model error in our constrained calculation of ΔT_{2x} is Gaussian with mean μ_{CS} (assumed to be zero) and variance σ_{CS}. These quantities are distinct from μ_{CS} and σ_{LGM} which represent the structural error in the modelling of the LGM constraint. We also apply this equation in its more general form (i.e. climate y_V, model output $g_V(\theta^*)$ and structural error mean μ_V and variance σ_V) to derive $2xCO_2$ and LGM probability distributions for other output variables in Section 8.

The structural error σ_{CS} in the calculation of ΔT_{2x} is arguably likely to be dominated by the assumption of a constant OL1 feedback parameter. Schneider von Deimling (2006) found a very close correlation between LGM tropical SST anomalies and ΔT_{2x} using CLIMBER-2. These results suggest the assumption of a constant feedback parameter introduces a 2σ structural error in ΔT_{2x} of only ~0.25°C. However, the correlation between LGM and $2xCO_2$ states was found to be substantially weaker in an AGCM coupled to a slab ocean (Annan et al 2005), suggesting a 1σ structural error of ~0.8°C is more appropriate. PMIP2 simulations (Masson-Delmotte 2006) suggest an approximately linear relationship between forcing and temperature change between LGM and $4xCO_2$ forcing. However, this result may be a reflection of averaging over differing model responses; Crucifix (2006) compared the results of the 4 PMIP2 GCMs which were applied to both LGM and $2xCO_2$ states and found that the assumption of constant feedback parameters for LGM and ΔT_{2x} may break down, primarily due to the non-linear response of subtropical shallow convective clouds to temperature change. We here apply a 1σ structural error $\sqrt{\sigma_{CS}} = 0.8$°C, noting that this range is greater that the standard deviation (±0.7°C) of the 19 GCM equilibrium climate sensitivities in IPCC (2007), differences which primarily reflect differing cloud and lapse rate feedbacks. A broader structural error assumption of $\sqrt{\sigma_{CS}} = 1.2$°C is also included for comparison.

Figure 8 is a scatterplot of ΔT_{2x} verses LGM tropical SST anomalies; open circles are the 894 MPC parameter vectors and filled circles are the subset of 480 LPC parameter vectors. The vertical lines represent the 1σ observational estimate of Ballantyne et al (2005). The dashed lines are the 2σ RMS deviation from a straight line fit to the LPC simulations. The 2σ uncertainty of ±0.9°C compares to ±0.25°C (Fig. 6 of Schneider von Deimling et al, 2006) and ±1.6°C (ACGM ensemble, Fig. 2 of Annan et al 2005); although our precalibration approach has captured much of the uncertainty associated with asymmetric responses to warming and cooling climate, the lack of a dynamic atmosphere inevitably fails to capture all of the uncertainty apparent in the AGCM ensemble. We note that the structural error term $\sqrt{\sigma_{CS}}$ (= 0.8°C) is primarily designed to allow for the asymmetric atmospheric feedbacks which GENIE-1 cannot capture.

7 Probability distribution for Climate sensitivity

We derive posterior distributions for climate sensitivity under a range of assumptions (A1 to A10), summarised in Table 4. The purpose here is to investigate the robustness of our conclusions with respect to the partially subjective choices that we are required to make in our Bayesian analysis. We note that such subjective choices are invariably required in a complex statistical analysis; one benefit of a Bayesian approach is to make these choices explicit and provide a quantification of their role. Our "best" estimate A7 (applying the assumptions described in section 6) is in bold face. The alternative analyses are:

A1) Neither LGM nor prior constraints are imposed (the calculation is derived from the MPC parameter set) and an allowance for structural error is not incorporated into the calibration (though we assume a small structural error of $\sqrt{\sigma_{CS}} = 0.2$°C in K_{LW1} which acts to smooth the posterior). Unconstrained GENIE-1 climate sensitivity peaks at 3.0°C, likely in the range 2.8 to 4.4°C. This assumption is (the smoothed) equivalent of the precalibrated climate sensitivity plotted in the histogram in Figure 2, and is plotted as the light orange line in the first panel of Figure 9.

A2) The introduction of priors (see Section 6) for CO_2 fertilisation (VPC) and isopycnal diffusivity (OHD) has little effect on ΔT_{2x}, reducing the most likely value to 2.9°C. This is dominantly a consequence of reduced photosynthesis and, presumably, the resulting increase in land surface albedo.

A3) The introduction of LGM constraints (still neglecting structural error) by incorporating the LPC priors and constraining with LGM tropical SST markedly narrows the uncertainty. The LGM constraint shifts the most probable climate sensitivity upwards to 3.5°C as less sensitive climates are generally less able to reproduce the observed LGM cooling.

A4) Introducing a structural error assumption of $\sqrt{\sigma_{LGM}} = 1.5$°C in LGM tropical SSTs in the calibration stage increases the most probable climate sensitivity to 3.7°C. This reflects the increased influence of extreme cooling responses (associated with increased sensitivity) in the long tail of the distribution, which are less strongly disfavoured under the assumption of a large model error.

A5) Introducing a structural error of $\sqrt{\sigma_{CS}} = 0.8$°C (the assumption of a constant feedback parameter K_{LW1}) (with $\sigma_{LGM} = 0$) substantially increases the uncertainty in ΔT_{2x}, but does not affect the peak of the distribution. The effect of this error term is to weaken the LGM constraint imposed on K_{LW1} and hence to broaden the estimate of ΔT_{2x}; it does not affect the probabilities ascribed to parameter vectors in the calibration stage and hence has little affect on the "peak-shifting" driven by the LGM constraint.

A6) The combined effect of both sources of structural error σ_{LGM} and σ_{CS} (A4 and A5) is a broadened distribution, shifted towards a higher climate sensitivity.

A7) A bias is introduced into the structural error at the calibration stage ($\mu = 0.6$°C) to reflect the neglect of dust and the resulting warm-bias in LGM tropical SSTs. We reduce our structural error assumption to $\sqrt{\sigma_{LGM}} = 1.0$°C, reflecting our increased confidence now that the structural bias due to the neglect of dust has been accounted for. The incorporation of a bias term shifts the probability distribution to lower

climate sensitivities; the "optimum" model response is shifted towards warmer LGM SSTs (which would be cooled by the presence of dust), thus favouring parameterisations which exhibit lower sensitivities. The introduction of dust biasing has little impact upon the calculated climate sensitivity as a consequence of the conservative structural error assumptions which serve to weaken the LGM constraint. *Assumption A7 represents our favoured assumption set for ΔT_{2x} as likely to lie between 2.6 and 4.4°C, with a peak probability at 3.6°C.*

A8) For comparison, the same assumptions are applied to the MPC parameter set. It is apparent that removing the LGM Antarctic plausibility test would largely reconcile the 90% confidence interval (1.6 to 4.7°C) with the CLIMBER-2 estimate of 1.2 to 4.3°C (Schneider von Deimling et al, 2006).

A9) For further comparison we apply the alternative LGM constraint of the East Antarctic SAT anomaly (9.0±2.0°C, Crucifix 2006) as favoured by Hargreaves et al (2007). To avoid double counting of the Antarctic SAT constraint, we here perform the Monte Carlo integration over the MPC parameter set (which is not filtered for LGM Antarctic plausibility). We assume an increased structural error of $\sqrt{\sigma_{LGM}} = 2$°C, reflecting additional uncertainty due to polar amplification, and an Antarctic dust-induced bias of $\mu = 1.0$°C (Schnieder von Deimling, 2006b). This analysis produces a similar climate sensitivity to the tropical SST constraint, peaking at 3.5°C and likely to lie between 2.6 and 4.5°C. We note that the application of the Antarctic constraint introduces additional uncertainties (especially given our simplified atmosphere), primarily due to changes in ice-sheet topography (Krinner and Genthon, 1998), but include this analysis as a useful validation of the robustness of our results.

A10) For further comparison, we include an SST constrained calculation with a more conservative structural error assumption for $K_{LW1}\ \sqrt{\sigma_{CS}} = 1.2$°C. This does not affect our estimate of the most probable climate sensitivity, but broadens the likely range to lie between 2.3 and 4.7°C.

8 Probability distributions of LGM and 2xCO_2 climate states

Figure 9 illustrates the climate state posterior distributions for LGM and 2xCO_2 climate states, comparing the unconstrained distributions (Assumption A1) with the fully constrained distributions (Assumption A7). These comparisons illustrate the combined effects of the LGM tropical SST constraint, allowing for structural error, and the data-driven parameter priors for CO_2 fertilization and isopycnal diffusivity.

For fully constrained calculations, the structural error for LGM air temperature is assumed to be $\sqrt{\sigma_V} = 0.8$ºC, the same value as was assumed for 2xCO_2, though likely more conservative as it does not rely upon the assumption of a constant feedback parameter. As we are likely to underestimate LGM cooling due to the neglect of dust, we introduce this bias through $\mu_V = 1.0$°C (Schneider von Deimling, et al 2006b). The resulting estimate for LGM cooling of 6.2°C, likely in the range 5.3 to 7.5°C, is similar to the CLIMBER-2 estimate (Schneider von Deimling et al 2006b) of 5.8 ± 1.4°C (2σ). The CLIMBER-2 result was reconciled with PMIP-2 simulations (4.1 ± 1.0°C, Masson-Delmotte *et al* 2006) by considering additional cooling of ~1.5°C due to the combined effects of dust and vegetation, both of which were neglected in the PMIP-2 study.

For other output no bias is assumed ($\mu_V = 0$), but structural error $\sqrt{\sigma_V}$ was applied for Atlantic overturning (1 Sv), Arctic/Antarctic sea-ice area (1 million km^2), vegetation carbon (25 GtC) and soil carbon (100 GtC). Structural error is more difficult to estimate for these distributions, so we simply apply these minimal values in order to smooth the posteriors. The justification for this is that we have attempted to allow for structural error in these quantities through our ensemble design. The fully constrained distributions are summarised quantitatively in Table 5. The unconstrained distributions also include a minimal structural error assumption. These values are identical to those above, with a value of $\sqrt{\sigma_V}$ = 0.2ºC for air temperature, which is applied as a smoothing term to both LGM and 2xCO_2 states. Aside from the smoothing effect of the structural error term, the unconstrained distributions are directly comparable to the frequency histograms in Figure 6.

Changes in land carbon storage are especially noteworthy. Under LGM conditions, the peak probability for land carbon storage change is a reduction by 470 GTC from modern values, likely in the range 330 to 700 GTC (this calculation assumes the complete removal of land carbon under ice-sheets). Under 2xCO_2, the change in equilibrium land carbon storage is of unclear sign, with a peak probability at 30 GTC, likely to lie in the range -160 to +350 GTC, with a 37% probability terrestrial carbon is reduced from modern values, so that land has turned from a sink to a source of atmospheric CO_2. These figures are sensitive to the constraint imposed by the prior distribution for CO_2 fertilisation (see Section 6). Assuming a uniform prior distribution for VPC from 0 to 700 ppm (Table 1), likely to overstate the effect of CO_2 fertilisation, the probability of a sink/source transition under elevated CO_2 is 24%. Note that additional constraints could be imposed through priors on other parameterisations, notably the respiration response to temperature.

Although the ensemble design has allowed a wide range of responses, it does not allow for all sources of structural error; the absence of a potential effect of Greenland melt on overturning and the inability to reproduce die-back of tropical forest under elevated CO_2 are two examples already noted. The assumption of a constant freshwater flux assumption (see Section 3) is especially noteworthy; GCM simulations (Zaucker and Broecker 1992) suggest an uncertainty of ±0.15 Sv in this assumption, corresponding to an uncertainty of ±3Sv in Atlantic overturning in GENIE-1 (Marsh et al 2004). Accordingly, the posteriors in Figure 9 and Table 5 are likely to provide an under-estimate of the true uncertainty.

Global average air temperature and sea-ice coverage are constrained primarily through the LGM SST constraint. Vegetation and soil carbon are primarily constrained through the prior applied to CO_2 fertilisation which reduces the likely response to changes in atmospheric CO_2 concentrations. Atlantic overturning is primarily constrained though the prior applied to isopycnal diffusivity as weakening of Atlantic overturning (both in LGM and 2xCO_2 states) is more likely at the low values of isopycnal diffusivity favoured by the prior.

Although the constraints have served to narrow the uncertainty in the LGM global air temperature anomaly, they have not narrowed the uncertainty in climate sensitivity (although the most probable climate sensitivity is shifted to higher values). This is a consequence of the structural error ($\sqrt{\sigma_{CS}}$ = 0.8°C) applied to the assumption of a

constant OLR feedback parameter (see Section 6) which ensures that the climate sensitivity is not over-constrained by the LGM state (Crucifix 2006).

9 Summary and Conclusions

We have designed a large parameter set with the purpose of maximising the range of modelled feedback response in an effort to overwhelm the variance arising from structural error, as suggested by Rougier et al (in preparation). The ensemble was achieved by building deterministic emulators for five different aspects of the climate state, and then using a statistical filtering process known as Approximate Bayesian Computation to find modern plausible parameter sets. This approach proved remarkably successful in the objective of producing weakly constrained parameter vectors, resulting in a wide range of plausible climate states, centred upon the modern climate state. The complex precalibration procedure was required in view of the broad input ranges applied to 25 parameterisations, attempting to jointly address the major sources of uncertainty in each of the four modelled Earth system components; whilst only 1% of the 1,000 simulations from a maximin Latin hypercube design satisfied modern plausibility, more than 90% of simulations satisfied this requirement after the ABC-emulator filtering. The resulting parameter set is likely to have potential GENIE-1 applications elsewhere.

The range of responses exhibited by GENIE-1 with this parameter set encompasses most of the behaviour seen in multi-model GCM ensembles, notably displaying uncertainty in the sign of the change in Atlantic overturning in response to LGM boundary conditions. This suggests that the uncertainty in the response seen in GCMs (Weber et al 2007) may derive from parametric uncertainty rather than reflecting fundamental differences between models.

The emulation of climate sensitivity enables us to investigate the contribution of individual parameters to uncertainty. Whilst the uncertainty is unsurprisingly dominated by the atmosphere (±0.93°C), uncertainties in vegetation contribute ±0.32°C, with ocean ±0.24°C and sea-ice ±0.14°C.

In order to derive probability distributions for a range of Earth System responses, we have applied the analysis of Rougier (2007) to the ensembles of modern, LGM and $2xCO_2$ climate states. The LGM provides a paleodata constraint which we apply, together with data-based informative prior distributions, incorporating estimates of additional structural error, including an allowance for the bias introduced by the neglect of dust. Although our approach has not narrowed the uncertainty in climate sensitivity – our assumption of a structural error in the OLR feedback parameterisation that is greater than the variability of multi-model GCM comparisons ensures that this cannot be the case – our results indicate that LGM constraints imply a slight increase in the most probable value for ΔT_{2x} to 3.6°C, very likely to lie in the range 2.0 to 5.0°C. This compares to the CLIMBER-2 LGM constrained range of 1.2 to 4.3°C (Schneider von Deimling 2006), the upper limit of which was raised to 5.3°C when an allowance for structural uncertainty was incorporated. The increased lower limit of 2.0°C in GENIE-1 arises because GENIE-1 fails to produce plausible LGM Antarctic temperature anomalies (6-12°C) with climate sensitivity below ~2.5°C (see Figure 8); removing the LGM Antarctic plausibility constraint produces a GENIE-1 climate sensitivity very likely in the range 1.6 to 4.8°C. The increased upper limit in

GENIE-1 (with respect to CLIMBER-2) is at least in part due to the additional uncertainty introduced into the ensemble through the precalibration design.

We provide quantification for other important measures of the response to climate change, both in response to LGM cooling and $2xCO_2$ warming. These responses are summarised in Table 5 and in Figure 9, which compares the unconstrained modern-plausible distributions (assumption A1) with the fully constrained distributions (assumption A7). Notably, we calculate a most probable LGM cooling of 6.2°C, likely to lie in the range 5.3 to 7.5°C. We calculate a reduction in LGM land carbon storage likely to lie in the range 330 to 700 GTC. Change in $2xCO_2$ land carbon storage is of uncertain sign, with a probability of 37% that land carbon turns from a sink to a source of atmospheric CO_2.

Acknowledgements

This work was funded by the U.K. Natural Environment Research Council (QUEST-DESIRE, Quaternary QUEST and RAPID UK THC MIP), the U.K. Engineering and Physical Sciences Research Council (Managing Uncertainty in Complex Models project, MUCM) and the Leverhulme Trust. We are grateful for the thorough reviews of both referees which have greatly helped to strengthen the paper and to Jonathan Rougier for several very useful discussions.

References

Annan JD, Hargreaves JC, Ohgaito R, Abe-Ouchi A, Emori S (2005) Efficiently Constraining Climate Sensitivity with Ensembles of Paleoclimate Simulations. SOLA 1:181-184. Doi: 10.2151/sola.2005-047

Annan JD and Hargreaves JC (2006) Using multiple observationally-based constraints to estimate climate sensitivity. Geophysical Research Letters 33: L06704. Doi: 10.1029/2005GL025259

Ballantyne AP, Lavine M, Crowley TJ, Liu J, Baker PB (2005) Meta-analysis of tropical surface temperatures during the last Glacial Maximum. Geophysical Research Letters 32: L05712. Doi: 10.1029/2004GL021217

Berger A (1978) Long term variations of caloric insolation resulting from the Earth's orbital elements. Quaternary Research 9: 139-167

Beaumont MA, Zhang W, Balding DJ (2002) Approximate Bayesian Computation in Population Genetics. Genetics 162: 2025-2035

Claquin T et al (2003) Radiative forcing of climate by ice-age atmospheric dust. Climate Dynamics 20: 193-202. DOI: 10.1007/s00382-002-0269-1

Colman R, McAvaney B (2009) Climate feedbacks under a broad range of forcing. Geophysical Research Letters 36: L01702 doi:10.1029/2008GL036268

Crucifix M (2006) Does the Last Glacial Maximum constrain climate sensitivity? Geophysical Research Letters 33:L18701 Doi: 10.1029/2006GL027137

Edwards NR and Marsh R (2005) Uncertainties due to transport-parameter sensitivity in an efficient 3-D ocean-climate model. Climate Dynamics 24: 415-433. Doi: 10.1007/s00382-004-0508-8

Ferreira D, Marshall J, Heimbach P (2005) Estimating eddy stresses by fitting dynamics to observations using a residual-mean ocean circulation model and its adjoint. Journal of Physical Oceanography 35: 1891-1910

Friedlingstein P et al (2006) Climate-Carbon Cycle Feedback Analysis: Results from the C^4MIP Model Intercomparison. Journal of Climate 19: 3337-3353

Hargreaves JC, Abe-Ouchi A, Annan JD (2007) Linking glacial and future climates through and ensemble of GCM simulations. Climate of the Past 3: 77-87

Krinner G and Genthon C (1998) GCM simulations of the Last Glacial Maximum surface climate of Greenland and Antarctica. Climate Dynamics 14: 741-758

Lea DW (2004) The100,000-Yr Cycle in Tropical SST, Greenhouse Forcing, and Climate Sensitivity. Journal of Climate 17: 2170

Lenton TM and Huntingford C (2003) Global terrestrial carbon storage and uncertainties in its temperature sensitivity examined with a simple model. Global Change Biology 9: 1333-1352

Lenton TM, Williamson MS, Edwards NR, Marsh R, Price AR, Ridgwell AJ, Shepherd JG, Cox SJ, The GENIE team (2006) Millennial timescale carbon cycle and climate change in an efficient Earth system model. Climate Dynamics 26: 687-711. Doi: 10.1007/s00382-006-0109-9

Lunt DJ, Williamson MS, Valdes PJ, Lenton TM, Marsh R (2006) Comparing transient, accelerated, and equilibrium simulations of the last 30,000 years with the GENIE-1 model. Climate of the Past 2: 221-235

Marsh R, Yool A, Lenton TM, Gulamali MY, Edwards NR, Shepherd JG, Krznaric M, Newhouse S, Cox SJ (2004) Bistability of the thermohaline circulation identified through comprehensive 2-parameter sweeps of an efficient climate model. Climate Dynamics 23: 761-777

Masson-Delmotte V, Kageyama M, Braconnot P, Charbit S, Krinner G, Ritz C, Guilyardi E, Jouzel J, Abe-Ouchi A, Crucifix M, Gladstone RM, Hewitt CD, Jitoh A, LeGrande AN, Marti O, Merkel U, Motoi T, Ohgaito R, Otto-Bliesner B, Peltier WR, Ross I, Valdes PJ, Vettoretti G, Weber SL, Wolk F, Yu Y (2006) Past and future polar amplification of climate change: climate model intercomparisons and ice-core constraints. Climate Dynamics 26: 513-529 doi:10.1007/s00382-006-0109-9

Matthews HD and Kaldeira K (2007) Transient climate-carbon simulations of planetary geoengineering. Proceedings of the National Academy of Sciences of the United States of America 104: 9949-9954. Doi: 10.1073/pnas.0700419104

Murphy JM, Booth BBB, Collins M, Harris GR, Sexton DMH, Webb MJ (2007) A methodology for probabilistic predictions of regional climate change from perturbed physics ensembles. Philosophical Transactions of the Royal Society A 365: 1993-2028

Olsen JS, Watts JA, Allison LJ (1985) World major ecosystem complexes ranked by carbon in live vegetation. NDP-017, Carbon Dioxide Information Analysis Centre, Oak Ridge National Laboratory, Oak Ridge, Tennessee.

Peng CH, Guiot J, van Campo E (1998) Estimating changes in terrestrial vegetation and carbon storage: using palaeoecological data and models. Quaternary Science Reviews 17: 719-735

Peltier WR (1994) Ice age paleotopography. Science 265: 195-201

R Development Core Team (2004) R: A Language and Environment for Statistical Computing, R foundation for Statistical Computing, Vienna, Austria ISBN 3-900051-00-3, http:/www.R-project.org

Rougier J (2007) Probabilistic inference for future climate using an ensemble of climate model evaluations. Climatic Change 81: 247-264 Doi: 10.1007/s10584-006-9156-9

Rougier J, Cameron D, Edwards NR, Price AR (in preparation) Precalibrating an intermediate complexity climate model (EMIC)

Santner T, Williams B, Notz W (2003) The Design and Analysis of Computer Experiments. New York: Springer

Saltelli A, Chan K, Scott M (2000) Sensitivity Analysis. New York: Wiley

Schneider von Deimling T, Held H, Ganopolski A, Rahmstorf S (2006) Climate sensitivity estimated from ensemble calculations of glacial climate. Climate Dynamics 27: 149-163. Doi: 1007/s00382-006-0126-8

Schneider von Deimling T, Ganopolsky A, Held H and Rahmstorf S (2006b) How cold was the Last Glacial Maximum? Geophysical Research Letters 33: L14709 doi:10.1029/2006GL026484

Stainforth DA et al (2005) Uncertainty in predictions of the climate response to rising levels of greenhouse gases. Nature 433: 403-406

Thompson SL and Warren SG (1982) Parametization of Outgoing Infrared Radiation Derived from Detailed Radiative Calculations. Journal of the Atmospheric Sciences 39: 2667-2680

Venables WN and Ripley BD (2002) Modern Applied Statistics with S. New York: Springer-Verlag, fourth edition

Webb MJ et al (2006) On the contribution of local feedback mechanisms to the range of climate sensitivity in two GCM ensembles. Climate Dynamics 27: 17-38 Doi: 10.1007/s00382-006-0111-2

Weber SL, Drijfhout SS, Abe-Ouchi A, Crucifix M, Eby M, Ganopolski A, Murakami S, Otto-Bliesner B, Peltier WR (2007) The modern and glacial overturning circulation in the Atlantic ocean in PMIP coupled model simulations. Climate of the Past 3: 51-64

Williamson MS, Lenton TM, Shepherd JG, Edwards NR (2006) An efficient numerical terrestrial scheme (ENST) for Earth System Modelling. Ecological Modelling 198: 362-374. Doi: 10.1016/j.ecolomodel.2006.05.07

Wullshleger SD, Post WM, King AW (1995) On the potential for a CO_2 fertilization effect in forests: estimates of the biotic growth factor based on 58 controlled exposure studies, in: Biotic Feedbacks in the Global System: Will the Warming Feed the Warming? Woodwell GM and Mackenzie FT (eds) Oxford: Oxford University Press pp 85-107

Zaucker F and Broecker WS (1992) The influence of atmospheric moisture transport on the freshwater balance of the Atlantic drainage basin: General Circulation Model simulations and observations. Journal of Geophysical Research 97: 2765-2773

Figures

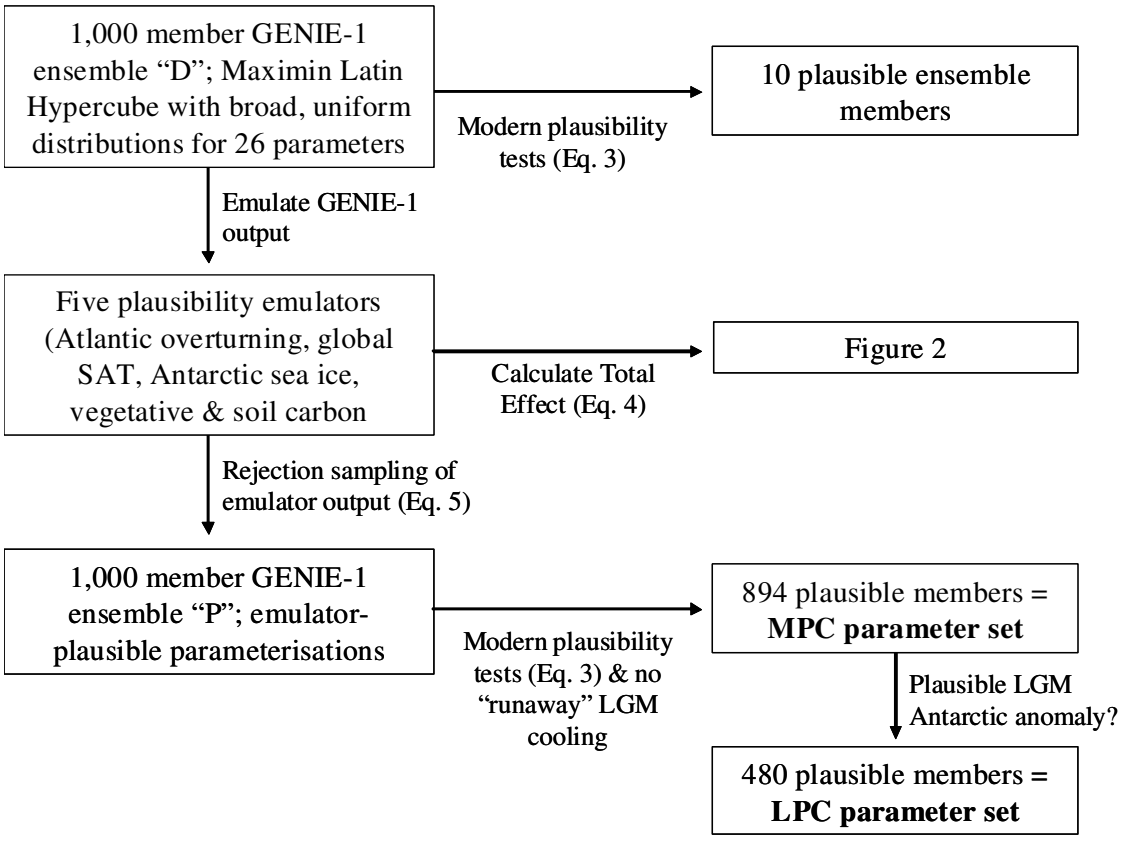

Fig. 1 Flow chart of the precalibration approach (section 3) used to construct the MPC and LPC parameter sets.

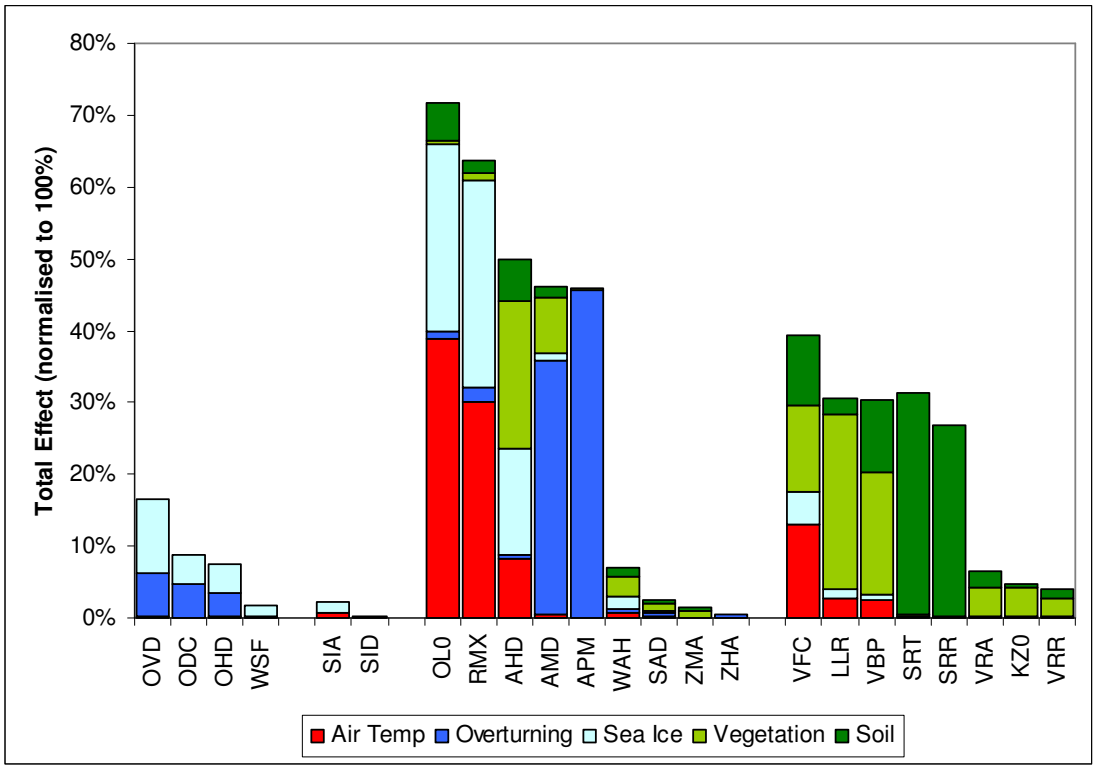

Fig. 2 The relative role of parameters in determining the modern state. The total effect of each parameter (the expectation of the variance which remains when all other parameters are known) is calculated for each emulator. These are normalised to 100% to approximate the percentage contribution of each parameter to the variance of each emulator as an illustration of which parameters drive uncertainty in the modern state.

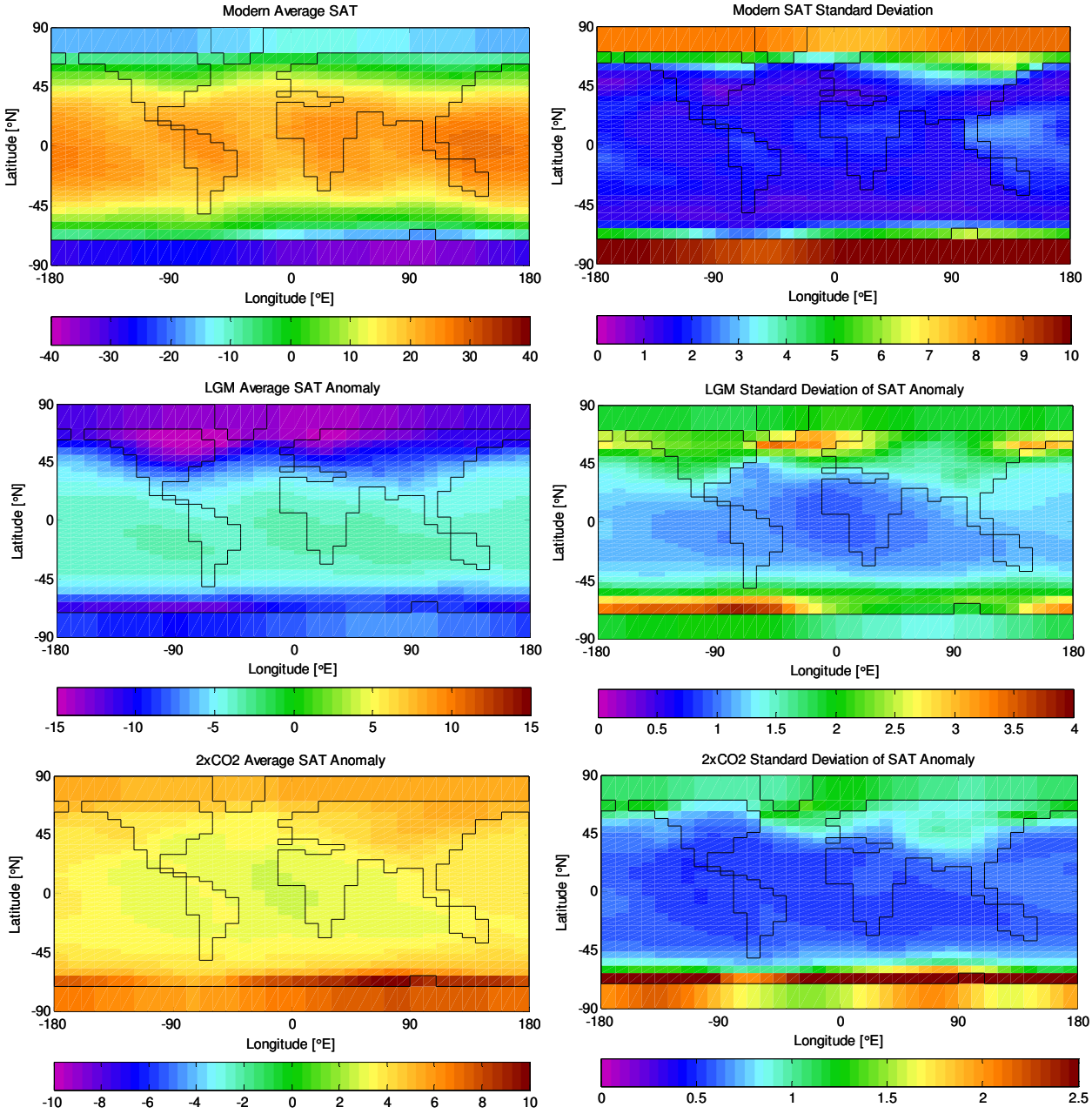

Fig. 3 Surface Air Temperature (°C). LPC ensemble averages (left) and standard deviations (right). From top to bottom the plots illustrate the modern state, the LGM anomaly and the $2xCO_2$ anomaly.

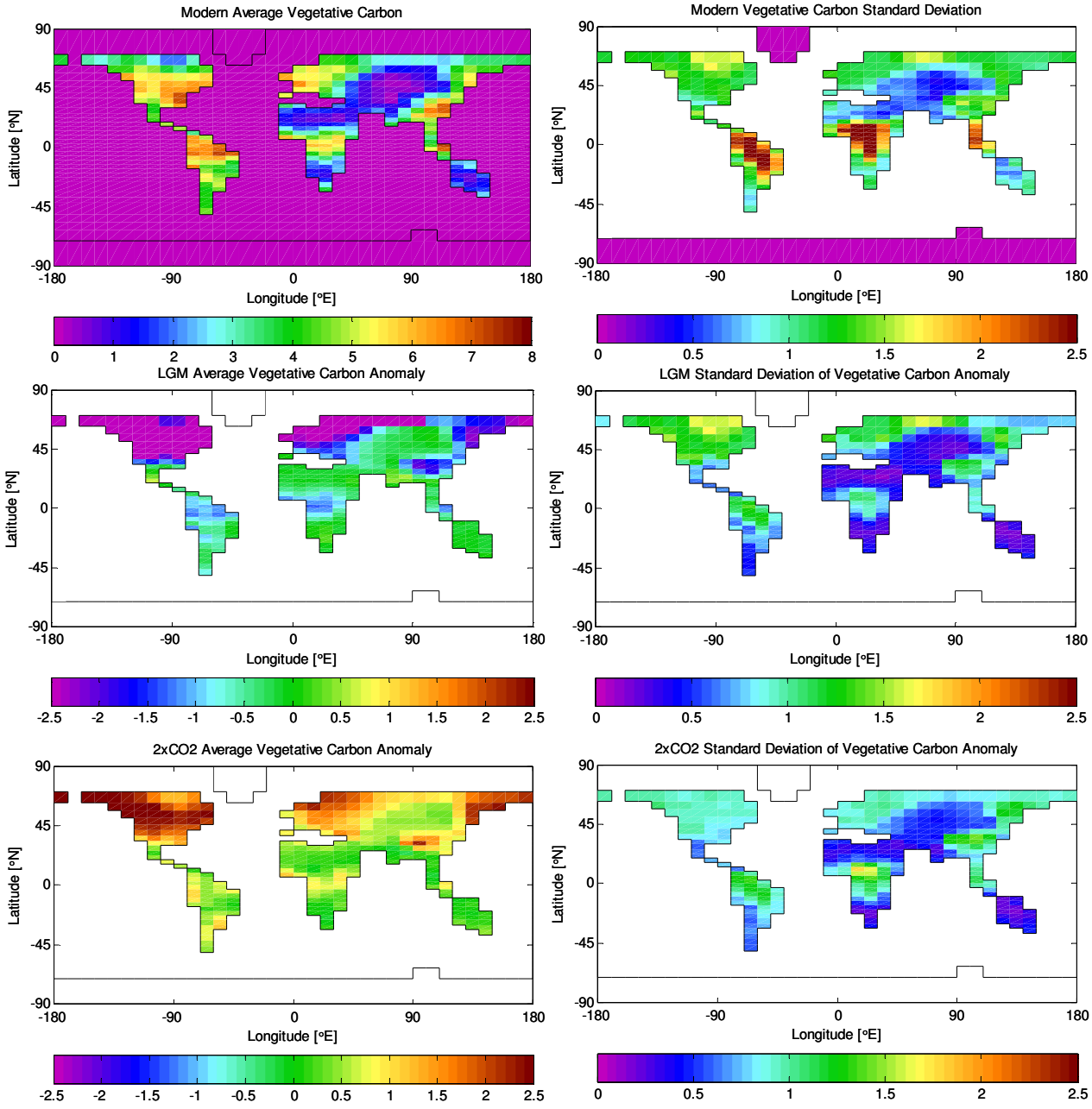

Fig. 4 Vegetation carbon ($kgCm^{-2}$). LPC ensemble averages (left) and standard deviations (right). From top to bottom the plots illustrate the modern state, the LGM anomaly and the $2xCO_2$ anomaly.

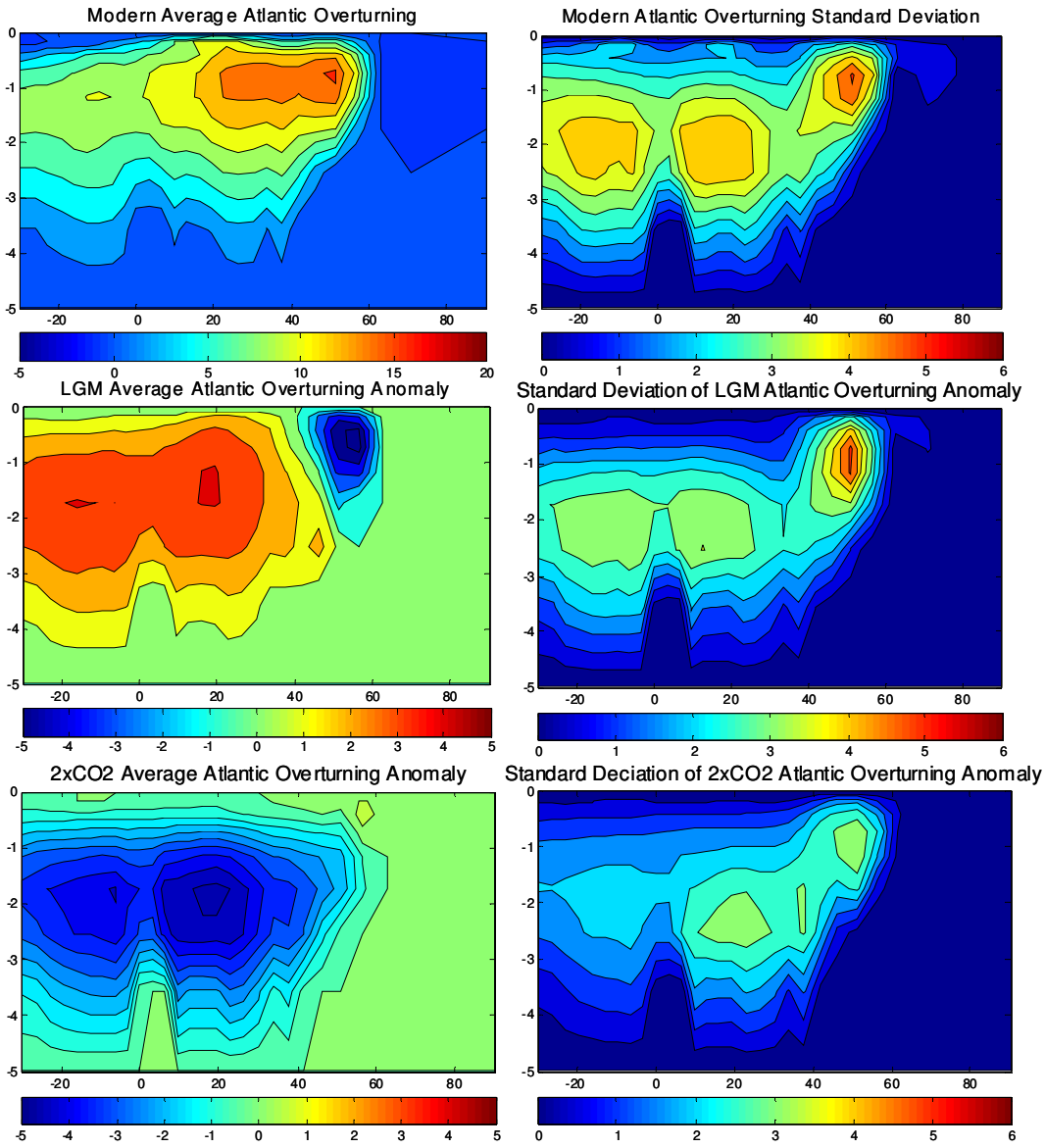

Fig. 5 Atlantic Overturning stream function (Sv). LPC ensemble averages (left) and standard deviations (right). From top to bottom the plots illustrate the modern state, the LGM anomaly and the $2xCO_2$ anomaly.

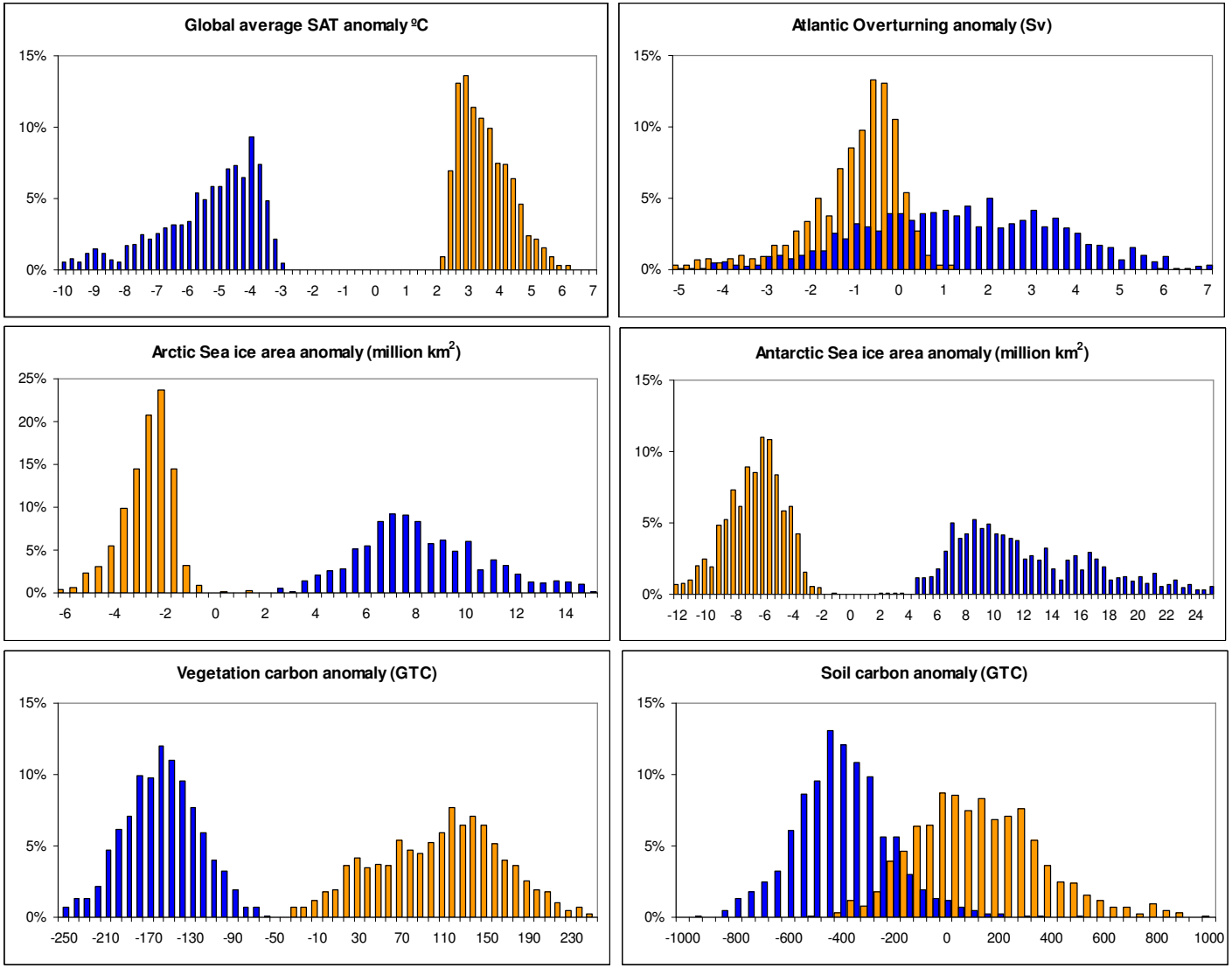

Fig. 6 MPC Frequency histograms for LGM anomalies (blue) and 2xCO_2 anomalies (orange). Some extreme "outlying" values are omitted for ease for presentation but are discussed in the text.

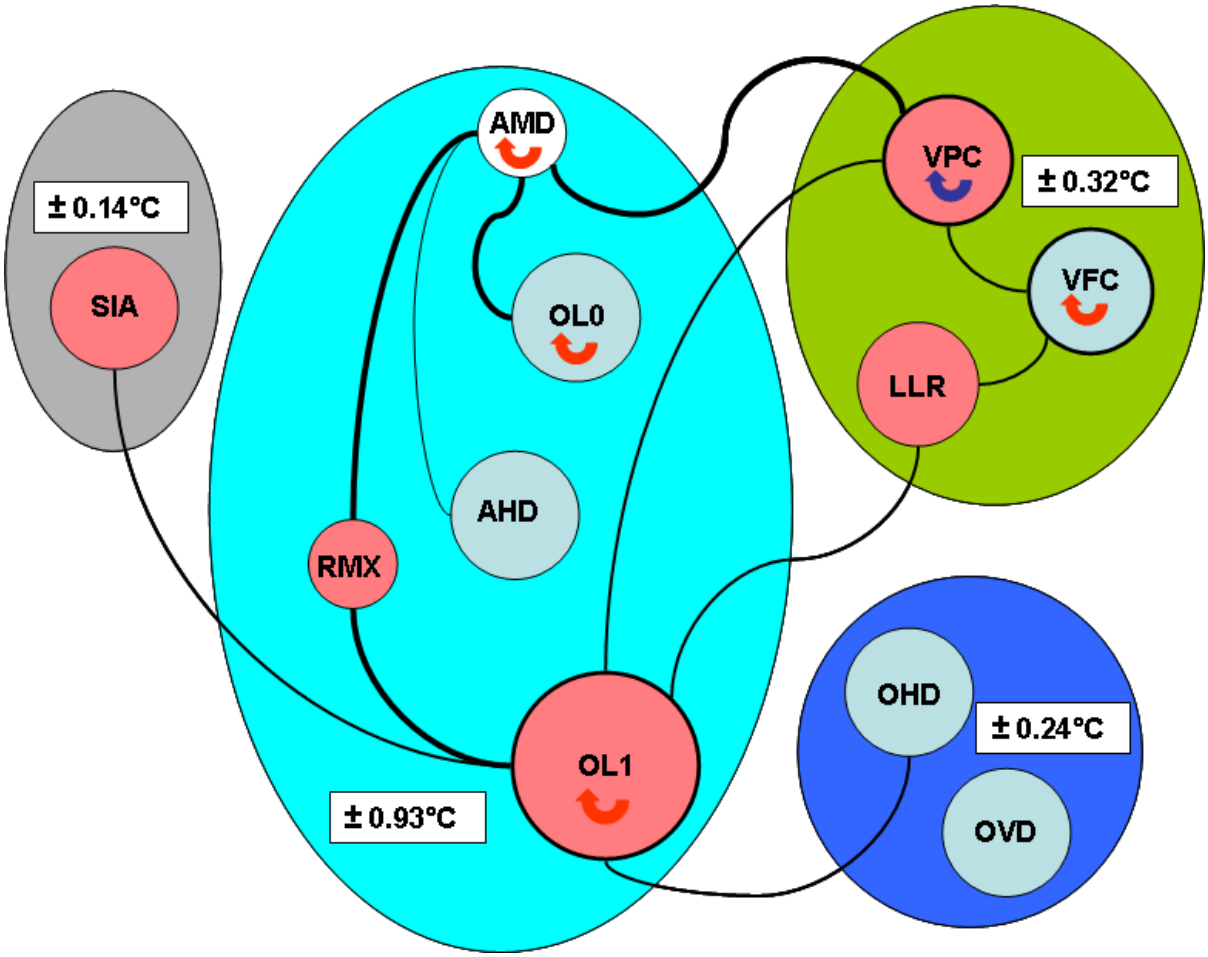

Fig. 7 The climate sensitivity emulator. The four GENIE modules are grouped separately: EMBM atmosphere (turquoise), GOLDSTEIN ocean (blue), sea ice (grey) and ENTS vegetation (green). The filtering process to select terms is described in the text. The 1σ error contributions for each module are approximated as the square root of the sum of the total effects $\sqrt{\Sigma V_T}$ of the parameterisations in that module (Table 4). Red circles are positive linear terms which contribute more than the standard error of the emulator when the parameter is varied across its input range. Blue circles are negative linear terms. Medium sized circles contribute more than twice the standard error of the emulator. Large circles (OL1) contribute more than four times the standard error. Lines represent interactions which contribute more than the standard error; thick lines contribute more than twice the standard error. Reverse arrows represent quadratic terms which are positive (red) or negative (blue).

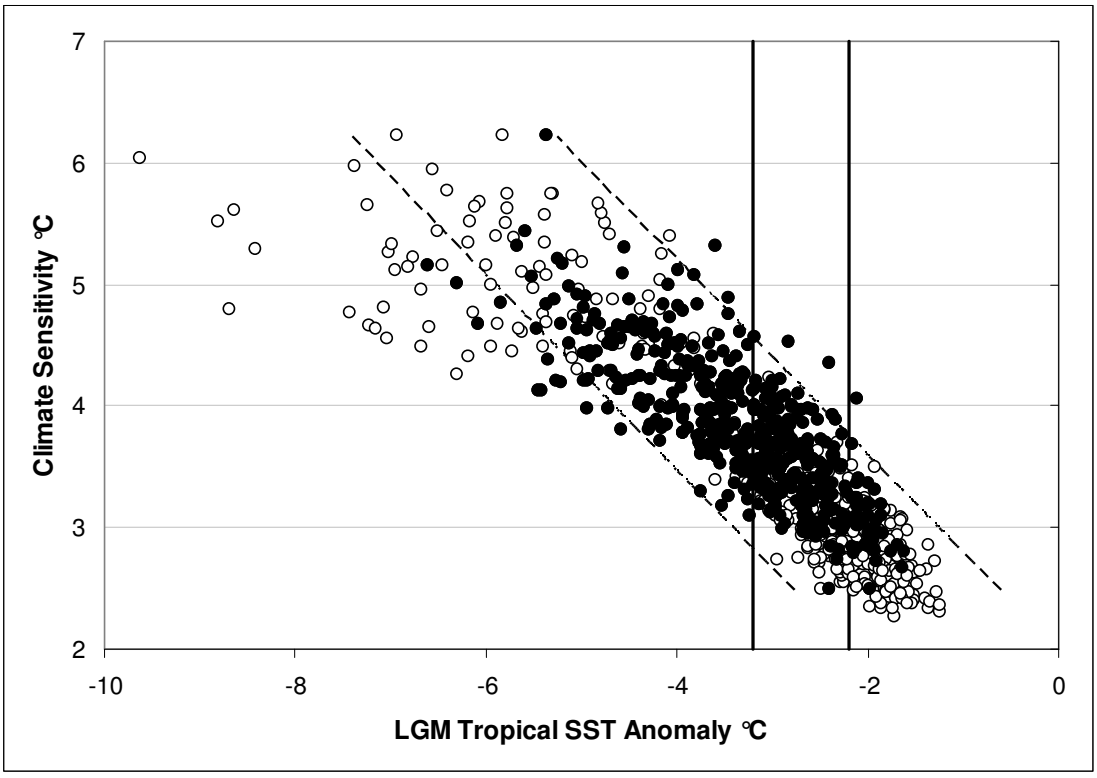

Fig. 8 Scatterplot of Climate sensitivity against LGM tropical SST anomaly. Open circles are the MPC parameter set and filled circles the LPC parameter set (a subset of MPC but filtered for LGM Antarctic SAT plausibility). Solid vertical lines are the 1σ range of the multi-proxy paleodata (Ballantyne et al 2005) applied as the LGM constraint. Dashed lines are the 2σ RMS scatter about a straight line fit to the 480 LPC simulations, representing an uncertainty of ±0.9C.

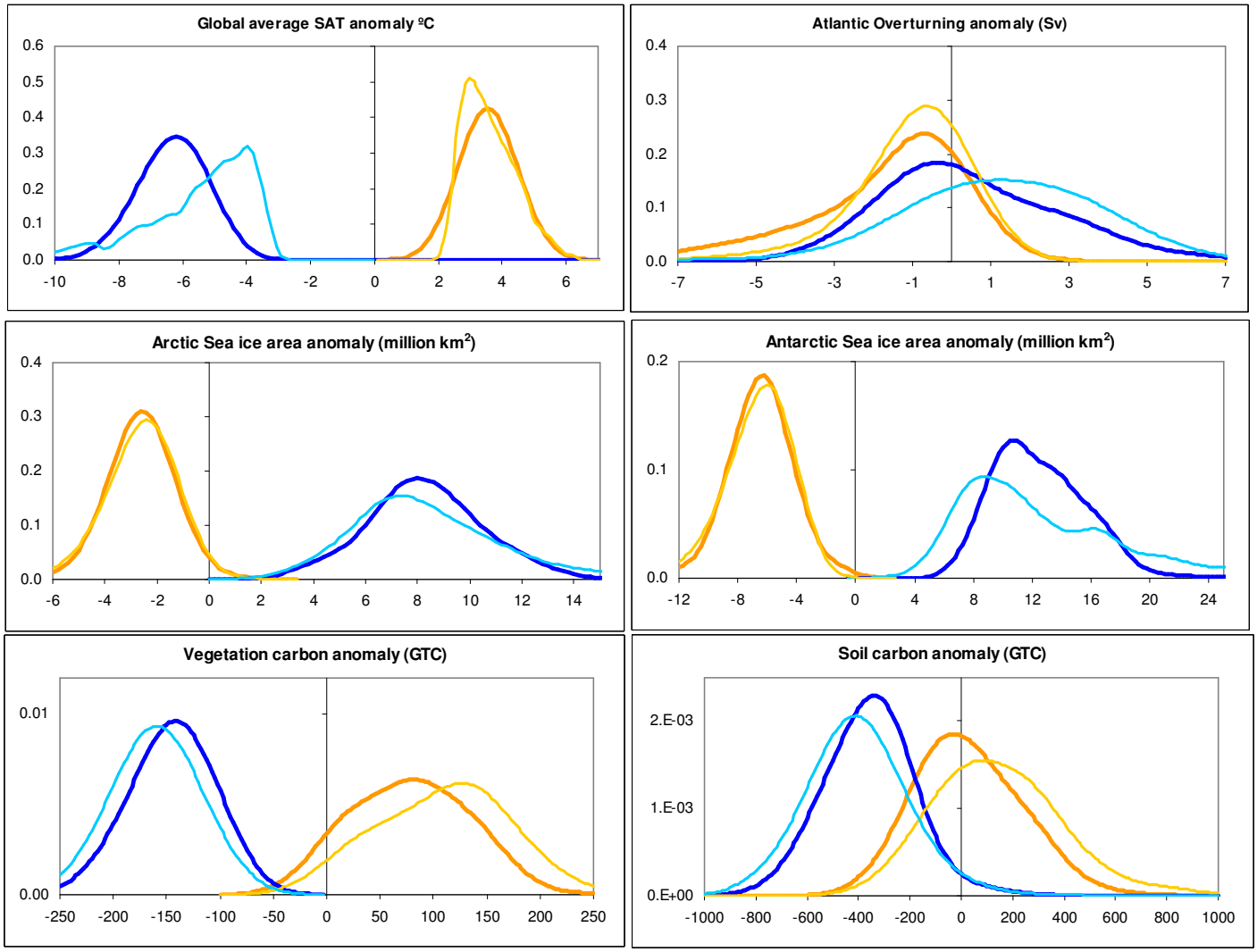

Fig. 9 Probability distributions for LGM and 2xCO_2 climate states**.** LGM (blue) and 2xCO_2 (orange)**.** Light lines illustrate the unconstrained distributions (assumption A1) and dark lines the fully constrained posterior distributions (assumption A7).

Tables

Table 1 Ensemble parameters: 25 parameters were varied across the ranges detailed below. The parameters were incorporated into a uniformly spaced maximin Latin Hypercube for the initial ensemble (used to derive plausibility emulators) and retained as input bounds for the ABC-filtering process which derived the plausibility parameter set. References for the parameters can be found in a) Edwards and Marsh (2005), b) Lenton et al (2006), c) Thompson and Warren (1982), d) Matthews and Caldeira (2005), e) Williamson et al (2006), f) Wullschleger et al (1995) and g) Lenton and Huntingford (2003).

Parameter description	**Ref**	**Minimum**	**Maximum**
OHD, Ocean isopycnal diffusivity (m^2s^{-1})	a	300	9,000
OVD, Ocean diapycnal diffusivity (m^2s^{-1})	a	$2x10^{-6}$	$2x10^{-4}$
ODC, Ocean friction coefficient ($days^{-1}$)	a	0.5	5.0
WSF, Wind scale coefficient	a	1	3
SID, Sea ice diffusivity (m^2s^{-1})	a	300	25,000
SIA, Sea ice albedo		0.5	0.7
AHD, Atmospheric heat diffusivity (m^2s^{-1})	a	$1x10^6$	$5x10^6$
WAH, Width of atmospheric heat diffusivity (Radians)	a	0.5	2.0
SAD, Slope of atmospheric diffusivity	a	0	0.25
AMD, Atmospheric moisture diffusivity (m^2s^{-1})	a	$5x10^4$	$5x10^6$
ZHA, Heat advection factor	a	0	1
ZMA, Moisture advection factor	a	0	1
APM, Atlantic-Pacific freshwater flux (Sv)	a	0.05	0.64
RMX, Relative humidity threshold for precipitation	b	0.6	0.9
OL0, K_{LW0} clear skies OLR reduction (Wm^{-2})	c	0	10
OL1, K_{LW1} OLR feedback ($Wm^{-2}K^{-1}$)	d	-0.5	0.5
VPC (k_{14}), photosynthesis half-saturation to CO_2 (ppmv)	e, f	0	700
VFC (k_{17}), fractional vegetation dependence on C_{veg} ($kgCm^{-2}$)	e	0.2	1.0
VBP (k_{18}), base rate of photosynthesis ($kgCm^2year^{-1}$)	e	3.0	5.5
VRA (k_{20}), vegetation respiration activation energy ($Jmol^{-1}$)	e, g	24,000	72,000
VRR (k_{24}), vegetation respiration rate ($year^{-1}$)	e	0.16	0.3
LLR (k_{26}), leaf litter rate ($year^{-1}$)	e	0.075	0.260
SRR (k_{29}) soil respiration rate ($year^{-1}$)	e	0.1	0.3
SRT (k_{32}), soil respiration activation temperature (K)	e, g	197	241
KZ0, roughness dependence on C_{veg} ($m^{-3}kgC$)	e	0.02	0.08
FFX, dummy variable		N/A	N/A

Table 2 The 5 plausibility metrics. The Plausibility test R_k describes the range of values which are accepted as "plausible" realisations of GENIE-1. The ABC test R_k^* describes the range of values which are accepted as potentially plausible realisations of the emulators: parameter sets found to satisfy all 5 ABC criteria (Equation 5) were supplied as input to GENIE-1 and accepted as plausible if GENIE-1 output satisfied all 5 plausibility criteria (Equation 3). The averages, standard deviations and ranges of the GENIE output from the 894 MPC parameter sets are provided in the third and fourth columns.

		Plausibility test R_k	ABC test R_k^*	MPC Ensemble Mean & 1σ Deviation	MPC Ensemble Range
Ocean	Atlantic overturning stream function Sv	10 to 30	13 to 19	18 ± 3	10 to 29
EMBM	Global SAT °C	12 to 16	13.5 to 15.5	14.1 ± 0.7	12 to 16
Sea ice	Antarctic Sea-ice area million km^2	3 to 20	8 to 12	9 ± 3	3 to 19
Vegetation	Total carbon GTC	300 to 700	350 to 550	440 ± 60	300 to 610
Soil	Total carbon GTC	750 to 2,000	1,100 to 1,400	1250 ± 170	840 to 1,880

Table 3 The contribution of individual parameters to the uncertainty in climate sensitivity of GENIE-1. Uncertainty is quoted in units of ºC. Calculations are presented which integrate over the Latin Hypercube parameter set (to illustrate uncertainty given our initial uniform priors) and over the LPC parameter set (to illustrate constraints imposed by modern and LGM plausibility). The square root of the total effect $\sqrt{V_T}$ of each parameter is tabulated as a measure of the contribution of that parameter to uncertainty in ΔT_{2x}. The contribution of individual Earth System modules is approximately quantified as $\sqrt{\Sigma V_T}$, summing over the parameters for the respective module.

	Hypercube (uniform priors)				**LPC**
		Test Robustness			
	Cubic Emulator	Convergence Test	Cubic 600 Emulator	Quadratic Emulator	**Cubic Emulator**
OHD	**0.13**	0.13	0.14	0.12	**0.11**
OVD	**0.14**	0.14	0.15	0.14	**0.08**
ODC	**0.06**	0.06	0.07	0.07	**0.04**
WSF	**0.13**	0.13	0.05	0.04	**0.06**
Total Ocean	**0.24**	0.24	0.23	0.20	**0.16**
SID	**0.05**	0.05	0.05	0.05	**0.02**
SIA	**0.13**	0.13	0.12	0.11	**0.14**
Total Sea-ice	**0.14**	0.14	0.13	0.12	**0.14**
AHD	**0.22**	0.22	0.19	0.24	**0.16**
WAH	**0.11**	0.11	0.11	0.13	**0.09**
SAD	**0.00**	0.00	0.00	0.03	**0.00**
AMD	**0.23**	0.23	0.11	0.15	**0.08**
ZHA	**0.06**	0.06	0.05	0.03	**0.04**
ZMA	**0.05**	0.05	0.04	0.05	**0.02**
APM	**0.06**	0.06	0.07	0.05	**0.04**
RMX	**0.15**	0.15	0.14	0.13	**0.09**
OL0	**0.25**	0.25	0.12	0.14	**0.12**
OL1	**0.81**	0.81	0.74	0.81	**0.61**
Total EMBM	**0.93**	0.93	0.81	0.89	**0.67**
VPC	**0.20**	0.20	0.18	0.20	**0.15**
VFC	**0.20**	0.20	0.19	0.19	**0.11**
VBP	**0.07**	0.07	0.10	0.10	**0.06**
VRA	**0.00**	0.00	0.00	0.05	**0.00**
VRR	**0.00**	0.00	0.00	0.03	**0.00**
LLR	**0.14**	0.13	0.15	0.15	**0.11**
SRR	**0.00**	0.00	0.00	0.00	**0.00**
SRT	**0.00**	0.00	0.00	0.02	**0.00**
KZ0	**0.06**	0.05	0.05	0.08	**0.05**
Total ENTS	**0.32**	0.32	0.32	0.34	**0.24**

Table 4 Bayes constrained climate sensitivity; Assumptions A1-A10.

	LGM Constraint	Parameter Priors	LGM Bias μ °C	Structural Error LGM Constraint $\sqrt{\Sigma_{LGM}}$ °C	Structural Error K_{LW1} extrapolation $\sqrt{\Sigma_{CS}}$ °C	Most Likely Climate Sensitivity °C	66% Confidence Interval (Range) °C	90% Confidence Interval (Range) °C
1	None	MPC	No	N/A	0.2	3.0	2.8 to 4.4 (1.6)	2.4 to 5.1 (2.7)
2	None	MPC & VPC, OHD	No	N/A	0.2	2.9	2.7 to 4.3 (1.6)	2.4 to 5.0 (2.6)
3	Plausibility & Tropical SST	LPC & VPC, OHD	No	0	0.2	3.5	3.0 to 3.9 (0.9)	2.8 to 4.2 (1.5)
4	Plausibility & Tropical SST	LPC & VPC, OHD	No	1.5	0.2	3.7	3.1 to 4.2 (1.1)	2.8 to 4.6 (1.8)
5	Plausibility & Tropical SST	LPC & VPC, OHD	No	0	0.8	3.5	2.6 to 4.3 (1.7)	2.0 to 4.9 (2.9)
6	Plausibility & Tropical SST	LPC & VPC, OHD	No	1.5	0.8	3.7	2.8 to 4.6 (1.8)	2.1 to 5.2 (3.1)
7	**Plausibility & Tropical SST**	**LPC & VPC, OHD**	**0.6**	**1.0**	**0.8**	**3.6**	**2.6 to 4.4 (1.8)**	**2.0 to 5.0 (3.0)**
8	Tropical SST	MPC & VPC, OHD	0.6	1.0	0.8	3.1	2.2 to 4.0 (1.8)	1.6 to 4.7 (3.1)
9	East Antarctic SAT	MPC & VPC, OHD	1.0	2.0	0.8	3.5	2.6 to 4.5 (2.0)	1.9 to 5.2 (3.4)
10	Plausibility & Tropical SST	LPC & VPC, OHD	0.6	1.0	1.2	3.6	2.3 to 4.7 (2.4)	1.4 to 5.6 (4.2)

Table 5 Posterior distributions for LGM and 2xCO_2 climate states

	Prior	Peak Probability	Likely range (66%)	Very likely range (90%)
LGM Anomaly				
Global SAT °C	-20 to 0	-6.2	-5.3 to -7.5	-4.6 to -8.3
Atlantic Overturning Sv	-20 to 20	-0.4	-2.0 to 2.6	-3.4 to 4.6
Arctic Sea Ice million km^2	0 to 20	8.0	6.1 to 10.3	4.4 to 12.1
Antarctic Sea Ice million km^2	0 to 30	10.7	9.3 to 15.5	7.7 to 17.9
Vegetation Carbon GTC	-400 to 0	-142	-106 to -186	-80 to -216
Soil Carbon GTC	-1,000 to 1,000	-340	-200 to -540	-70 to -670
Total Land Carbon GTC	-1,500 to 500	-470	-330 to -710	-180 to -850
2xCO2 anomaly				
Global SAT °C	0 to 10	3.6	2.6 to 4.4	2.0 to 5.0
Atlantic Overturning Sv	-25 to 15	-0.6	-4.0 to 0.2	-7.0 to 1.4
Arctic Sea Ice million km^2	-10 to 5	-2.6	-1.5 to -3.9	-0.6 to -4.8
Antarctic Sea Ice million km^2	-20 to 5	-6.4	-4.5 to -8.6	-2.9 to -10.3
Vegetation Carbon GTC	-200 to 400	82	16 to 133	-20 to 169
Soil Carbon GTC	-1,000 to 1,000	-30	-190 to 230	-320 to 390
Total Land Carbon GTC	-1,000 to 1,000	30	-160 to 360	-300 to 530